

Vulnerable Connectivity Caused by Local Communities in Spatial Networks

Yingzhou MOU* and Yukio HAYASHI¹

¹Japan Advanced Institute of Science and Technology, Nomi-city,
Ishikawa 923-1292, Japan.

Contributing authors: mouyingzhou@outlook.com;

Abstract

Local communities are widely observed in spatial networks. However, how such structure affects the vulnerability against malicious attacks remains unclear. This study investigates the impact of local communities on the robustness of connectivity by modeling planar infrastructure networks based on statistical population data. Our research reveals that the emergence of local communities is caused by spatial concentrations of nodes connected by short links, which significantly reduce the robustness. These results suggest that strategically establishing long-distance links provides a feasible solution to balance reliability and construction costs in infrastructure network design.

Keywords: Robustness of Connectivity, Local Community, Spatial Networks, Proximity Graphs, Population Distribution

1 Introduction

Community structure characterized by dense intra-community links and sparse inter-community bridge link is widely observed in various networks [1][2] including spatial networks [3][4][5][6]. Although there have been extensive researches on community

detection [7][8], it still be not elucidated how community structure affects the vulnerability against attacks. We take notice to that such a structure creates potential vulnerabilities: When critical bridge links are removed, the network tends to fragment into components [9]. Previous research has shown that artificially adding community structure can significantly weaken the robustness of connectivity in scale-free (SF) networks and Erdős-Rényi (ER) random graphs [10][11]. Unlike only topological SF networks and ER graphs, spatial networks are constrained by physical and geographical factors, which may be related to community structure. As examples of these factors, in densely populated areas, road networks require more intersections to meet traffic demands[12], while wireless communication networks[13] need more base stations to maintain service quality. Although it has been pointed out that *in a topological structure affected by geographical constraints on linking, the connectivity is weakened by constructing local stubs with small cycles* [14], the reason for this weakness remains unclear without considering the influence of community structure.

To address these gaps, we focus on road and communication networks as typical geographically constrained infrastructure networks. In constructing realistic spatial networks, we require reasonable data for locations of nodes. While there are many possible locations, the detail locations of nodes or links are not open usually for security reason to protect the using as potential targeted attacks. Therefore, we apply statistical population data of seven major urban areas in Japan as a realistic reference for determining node's locations. Moreover, since spatial networks embedded on the surface of Earth have many short links and tend to be planar because of geographical limitations and economic considerations, we consider relative neighborhood graph (RNG) [15] and Gabriel graph (GG) [16] as modeling of road and communication networks, respectively. RNG and GG are studied in computer science, and have similarities to road networks [17] or the self-organized biological transport networks such

as slime mould with interactions between the growing active zone and chemogradients [18].

This paper aims to investigate how local communities affect the robustness of connectivity in spatial networks. In particular, we show that spatial concentrations of nodes connected by short links lead to the emergence of local communities, which make spatial networks more vulnerable against node removals.

The remainder of this paper is organized as follows. In Section 2, we introduce proximity graphs of RNG and GG with short links, which construct spatial networks based on population data that determines node locations. We consider three node removal strategies (1) recalculated betweenness attacks (RB) [19] by removing high betweenness centrality nodes, (2) initial degree attacks (ID) [20] by removing high degree nodes, and (3) random failure (RF) [9] by removing nodes randomly. We focus on RB, since betweenness centrality-based attacks are the most effective for fragmenting the largest connected component (LCC) in networks with communities, while ID and RF are typical node removals for comparing with the above damages. In Section 3, we show how local communities emerge and affect the robustness of connectivity. In particular, we conclude that spatial networks with strong community structure weaken the robustness against intentional attacks and random failures.

2 Spatial Networks with Concentration of Nodes

We introduce the models of road and communication networks by considering four types of node's location, which give different strengths of local communities for investigating the robustness of connectivity against node removals.

2.1 Models of Spatial Networks

Real networks such as road or communication systems tend to be planar on the surface of Earth. Thus, they are constrained by physical and geographic limitations. Economic

considerations further reinforce this planarity for minimizing infrastructure investments. Moreover, the evolutionary nature of these networks by connecting neighbor nodes inherently leads to a planar structure through this proximity-based growth pattern. Based on this understanding, we introduce relative neighborhood graph (RNG) and Gabriel graph (GG) as models of road and communication networks, respectively, which are used to construct spatial networks. Note that RNG is a subgraph of GG and both of them are planar in proximity graphs with short links. These models have unique advantages for network analysis, particularly related to real-world population data as mentioned later.

RNG [15] and GG [16] are defined as follows. For a given set of nodes on a geographical space, two nodes are connected if no other node exists within a neighboring area of them. As shown in Figures 1 (a) (b), each shaded area is the intersection of two circles centered at two nodes with a radius equal to the distance between them.

RNG can be used to model road networks, because these links almost coincide with road segments in urban cities [21] [22]. GG has been used for modeling optical or ad-hoc wireless networks, because it resembles the structure of physical networks [16] [23] [24]. In particular, directional antennas are used in wireless networks with better beam power for linking [25]. In Figure 2, blue and orange shades represent strong area of directional beams, while the center circle represents the interference area. If other base station is located in this area with interference, connecting those two nodes is prohibited.

2.2 Node's Locations and Removal Strategies

Some studies focus on the strong correlation between population densities in cities and node's locations [4] [5]. In road networks, each cross point can be considered as a node, areas with higher population densities tend to have more nodes [12]. In communication networks, each base station can be considered as a node, such areas

with higher population densities require more nodes, since they maintain adequate signal coverage for communications [26] [27] [28].

Taking into account the correlation between population density and node's locations, we set three types of node's locations: Population (Pop.), Inverse Population (Inv.) and Uniform (Uni.). Here, the location of nodes are determined by the centers of meshes according to statistical population data mentioned in the next section. For Pop., the nodes are located according to densely populated points ranked from highest to lowest, representing an extreme case where investments are exclusively concentrated in the most populated areas. For Inv., the nodes are located according to sparsely populated points ranked from the lowest to the highest, representing a strategic utilization of extremely sparse areas because of lower land prices for constructing networks with links by asphalt pavements or cables and node equipments such as traffic lights or communication devices. For Uni., the nodes are located according to a uniformly at random distribution, which moderate the concentration of nodes in Pop. and Inv. as these extreme cases. In most cities, population density is uneven, there is mixing of sparse and dense node's locations in both Pop. and Inv.. The mixtures also occur in Uni. because of the spatial point process (SPP) theory [29]. Based on the SPP theory, the number of nodes in a given area follows a Poisson distribution, therefore there are mixtures of sparse and dense node's locations. These mixtures give local community structure as shown later. By connecting nodes on the locations of Pop., Inv., and Uni., spatial networks are constructed according to the previously described constraints of short links in RNG and GG shown in Figure 1. Moreover, as completely uniform without mixtures of dense and sparse node's locations, we consider the fourth type of node's locations on a 2D square lattice (2DL) [30] in matching the condition under a same $P(k)$ for comparing the robustness in 2DL and Pop., Inv., or Uni. networks. According to the slightly different degree distributions $P(k)$ as shown later obtained from Pop., Inv., and Uni. networks, we randomly assign the corresponding

number of links to each node on the 2DL. We assume that the other end of assigned link is free (unconnected) to perform the following two steps of trials for linking. The first trial is established by connecting free-ends between neighbor nodes on the lattice. When free-ends are remaining but its neighbor nodes have no available free-ends, the second trial is performed for connecting more distant nodes with free-ends available. Note that the 2DL is not planar with the second trial links.

On the other hand, as node removals, we consider three typical strategies: recalculated betweenness (RB) attacks [19], initial degree (ID) [20] attacks, and random failures (RF) [9]. In these strategies, nodes (and links connected to them) are removed one by one until q/N nodes are removed, where q and N denote the fraction of removed nodes and network size, respectively. Removed nodes are selected in decreasing order of degrees for ID attacks or betweenness centrality for RB attacks. Note that RB attacks recalculate betweenness centrality, while ID attacks select nodes according to the initial degree. Besides, RF is considered to enhance the difference between intentional attacks and random failures. We emphasize that RB has a strong affect on global fragmentation in networks with communities.

3 Effects of Community Structure on the Robustness

This section numerically shows important results for the robustness in the spatial networks. In subsection 3.1, we show the emergence of local communities in RNG and GG as modeling road and communication networks whose nodes are located by Pop., Inv., and Uni.. In subsections 3.2 and 3.3, we show that spatial concentrations of nodes connected by short links make local communities, which affect the robustness of connectivity against both intentional attacks and random failures.

3.1 Emergence of Local Communities

As real population data, the seven Japanese areas used in our study are Fukuoka, Hiroshima, Kyoto-Osaka (referred to as Keihan), Nagoya, Tokyo, Sendai, and Sapporo [31]. Each of them is divided into $500m \times 500m$ block meshes with totaling $(8 \times 10 \times 2 \times 3)^2 = 230,400$ blocks, while nodes are located at the centers of meshes. We select N nodes whose locations are based on Pop., Inv. and Uni., respectively, as mentioned in subsection 2.2 previously. To ensure that \sqrt{N} is an integer when constructing a 2DL for later comparison, we set $N = 100,1024$ and 10000 . Links between nodes are created by connection rules of RNG and GG as shown in Figure 1. Local communities emerge in such spatial networks.

To measure the strength of community structure, we introduce modularity Q [32] defined as:

$$Q = \frac{1}{2M} \sum_{ij} \left[A_{ij} - \frac{k_i k_j}{2M} \right] \delta(c_i, c_j),$$

where A_{ij} denotes the i, j element of adjacency matrix: $A_{ij} = 1$ if there is a link between nodes i and j , 0 otherwise. k_i and k_j are the degrees of them, respectively. M is the total number of links, c_i represents the community identifier to which node i belongs, $\delta(c_i, c_j)$ is an indicator function equal to 1 if nodes i and j belong to a same community, and 0 otherwise. We estimate c_i by using Louvain method [33]. A higher value of Q indicates a stronger community structure, where there are many intra-links however a few inter-links.

We explain the typical results of communities for Tokyo $N = 1024$ node networks as examples. For other cities, the results are shown in Supporting Information from S1 Fig. to S12 Fig.. Figures 3 and 4 show the communities for node's location based on Pop. and Inv. with short links created by RNG and GG. Since RNG is a subgraph of GG, the numbers of links in Figures 3 and 4 (a) are less than them in Figures 3 and 4 (b). Thus, the results of communities in RNG and GG networks are different.

Moreover, Figures 5 and 6 show the examples of communities for node’s location based on Pop. and Inv. after 10% nodes (and links connected to them) removals against RB attacks. The removal of nodes causes the network to break into disconnected components, particularly at the boundaries between different communities. This fragmentation is the most noticeable in densely populated areas. For all seven Japanese areas, Table 1 shows that both Pop. and Inv. have slightly higher Q values compared to Uni. for $N = 1024$. This trend is also observed for other sizes N in Supporting Information S6 Table and S7 Table. These results suggest that Pop. and Inv. networks have slightly stronger community structure than that of Uni. networks according to these spatial concentrations of nodes. Although Uni. has a slightly lower Q value than that of Pop. and Inv., it still maintains community structure obviously. Remember that from the SPP theory in subsection 2.2, there is a mixture of sparse and dense node’s locations, and contributes to the emergence of community structure even in Uni. networks.

3.2 Robustness of Connectivity Against Recalculated Betweenness Attacks

Robustness of connectivity plays a crucial role in complex networks for quantifying a network’s ability to maintain the functionality when subjected to intentional attacks or random failures, such as RB, ID and RF mentioned in subsection 2.2. As the measures, we use the robustness index R [34] and the critical fraction q_c [35]. Here, the robustness index R is the area under the curve of the LCC’s relative size $S^{1st}(q)/N$ against the fraction q of removed nodes. A higher R value indicates greater overall robustness of connectivity. The critical fraction q_c is the value of q at which the relative size $S^{2nd}(q)/N$ of the second LCC reaches its peak. It captures the critical point of structural change in a network. A higher q_c value suggests that the network can withstand more removals of nodes before substantial fragmentation. However,

R is a more precise measure because different R values are possible for rapidly and gradually decreasing curves of $S^{1st}(q)/N$ even with a same q_c . The combination of these two measures provides us with ways to observe not only how tenaciously a network maintains its connectivity against attacks but also when it reaches its breaking point.

Figures 7 show the remarkable relation between modularity Q and the robustness measures R against RB attacks. As Q increases (with stronger community structure), R decreases (with weaker robustness of connectivity) for all seven major Japanese areas with different node's locations. S36 Fig. and S37 Fig. in Supporting Information provide additional evidences of similar results in the networks with sizes $N = 100$ and $N = 10000$. In other words, as higher Q values with stronger community structure, the robustness becomes more vulnerable in the spatial network because of the limited number of inter-links (especially against RB attacks whose targets are the end-nodes of such bridges between communities).

We further investigate how community structure weakens the robustness of connectivity for these networks in explaining the details for examples of Tokyo 1024 node's networks. The results show that the spatial concentration of nodes creates strong community structure, which weaken the robustness. In Figures 8 and 9, it is common that both randomized networks and 2DL networks show rightward shifts in their curves as improving the robustness to the original networks. When $S^{2nd}(q)/N$ reaches its peak at q_c , the corresponding $S^{1st}(q)/N$ curve is rapidly decreased. We explain the details of comparisons in the following, where the R value is represented by the area under $S^{1st}(q)/N$ curve, and that the q_c value is indicated by the peak of $S^{2nd}(q)/N$ curve.

Figure 8 shows the robustness curves comparing the original networks (Pop., Inv., and Uni. node's connected by RNG or GG) with their degree-preserved randomized (rewired) counterparts where communities are eliminated. By comparing RNG

(Figures 8ac) and GG (Figures 8bd), we confirm that all curves in GG exhibit rightward shifts compared to their corresponding curves for RNG with same colors and line types. This rightward shift indicates higher robustness for GG as shown by both larger areas under the $S^{1st}(q)/N$ curves (higher R values) and delayed peaks in $S^{2nd}(q)/N$ curves (higher q_c values). Remember that RNG has fewer links than GG as the subgraph.

To investigate the effect of community structure on the robustness of connectivity, we compare the original networks (represented by RGB solid lines) with their randomized counterparts (shown as RGB dashed lines) in Figure 8a-d, where networks denoted by a same color line have an identical degree distribution $P(k)$ as shown in Figure 10. Green and red dashed lines (randomized Inv.) show significant rightward shifts compared to the corresponding solid lines (the original Pop., Inv.). These lines indicate that weaker community structure enhances the robustness. Similarly, blue dashed lines (randomized Uni.) show the improvement of robustness to its solid counterparts. In each of Figure 8a-d for the original networks (RGB solid lines), both green (Pop.) and red (Inv.) solid lines exhibit leftward shifts compared to blue lines (Uni.). It indicates that Uni. networks have higher robustness. These comparisons consistently show that stronger community structure (higher modularity Q values) lead to lower robustness, also as evidenced by increasing modularity Q values (see the differences for the original and randomized networks in Table 1). In other words, the limited number of inter-links create potential vulnerabilities against attacks. However, this relation becomes slightly complex in randomized networks with some exceptions: For RNG (Figure 8a), the green dashed lines (randomized Pop.) exhibit higher robustness than the blue dashed lines (randomized Uni.), while the red dashed lines (randomized Inv.) show lower robustness. For GG (Figure 8b), both green and red dashed lines have lower robustness than the blue dashed lines. With the exception of randomized

RNG networks, these cases suggest that a uniform distribution of nodes contributes to improved the robustness in Figure 8ab.

Figure 9 shows the robustness curves comparing the original networks with weaker community networks where nodes are relocated onto 2D lattices under same degree distributions of Pop., Inv., and Uni., respectively, to investigate how spatial concentrations of nodes affect the robustness of connectivity. In Figure 9a-d, the cyan solid lines (2DL-Uni.) show higher robustness than the blue solid lines (the original Uni.) as evidenced by both larger area under the $S^{1st}(q)/N$ curves (higher R value) and delayed peak in $S^{2nd}(q)/N$ curve (higher q_c value). Similar improvements of robustness are also observed, when comparing the yellow solid lines (2DL-Pop.) with the green solid lines (the original Pop.), and comparing the magenta solid lines (2DL-Inv.) with the red solid lines (the original Inv.). When comparing these networks, we observe a clear hierarchy in the robustness that correlates with the strength of community structure. As shown in Table 1, the original networks show stronger community structure while 2DL networks show weaker community structure. As exceptions in both randomized and relocated networks, RNG-Pop networks (in bold) have lower modularity Q than RNG-Uni networks, which may be attributed to RNG-Pop networks have more concentrated degree distributions than RNG-Uni networks. In Figures 8 and 9, randomized networks (RGB dashed lines) without communities have the highest robustness, followed by 2DL networks (Cyan-Yellow-Magenta, CYM solid lines), while the original networks (RGB solid lines) with strong communities have the lowest robustness. For instance, the blue dashed lines (randomized Uni.) show to be higher robust than the cyan solid lines (2DL-Uni.), which show to be even more robust than the blue solid lines (the original Uni.). Similar results can be observed in the comparisons between solid-green and dashed-yellow lines (Pop.), and between solid-red and dashed-magenta lines (Inv.). These comparisons reveal that weaker community structure through more homogeneous node's locations improves the robustness as shown by

the rightward shifts of CYM solid lines compared to that in the original networks. In summary, spatial networks with weaker community structure have higher robustness against RB attacks.

3.3 Robustness of Connectivity Against Initial Degree Attacks and Random Failures

We further investigate the robustness of connectivity against typical Initial Degree (ID) attacks and Random Failures (RF). For Uni. networks, we confirm that q_c values are almost identical to the analytical values [36] as shown in Tables 2 and 3. Table 2 shows the robustness index R and critical fraction q_c against ID attacks, while Table 3 shows the corresponding R and q_c values against RF. Note that a clear hierarchy exists as following the relation $R^{RB} < R^{ID} < R^{RF}$ and $q_c^{RB} < q_c^{ID} < q_c^{RF}$ (see S2 Table in Supporting Information for detailed comparison) in the robustness across different attack strategies.

In both ID attacks and RF, networks whose nodes are located according to Pop. and Inv. show lower R and q_c values than those to Uni. networks as similar to the results against RB attacks except some cases. As values with upper-triangles (Δ) in Tables 2 and 3, some networks based on Pop. and Inv. have higher robustness than those on Uni.. The reason may be caused by two factors: (1) Higher average degree $\langle k \rangle$ in RNG Pop. networks as shown in Table 4, which may provide additional alternative paths after node removals; (2) The presence of regular grid-like parts in certain regions of Pop. networks contributes to enhance the robustness against RF as shown in S15 Fig.. The effect of grid-like parts is explained as follows. In our study, all nodes are located limitedly at the centers of mesh blocks ($500\text{m} \times 500\text{m}$), rather than having arbitrary positions in a geographical space freely. When nodes are densely distributed in neighboring mesh blocks, as often occurs in Pop. networks, they tend to form grid-like parts. We quantify these grid-like parts by calculating the ratio of nodes that

have degree 4 with four neighbors of degree 4, which represents a typical local grid formation. As shown in Table 5, Pop. networks show notably higher ratio of such grid-like parts (ranging from 2.05% to 15.14% in RNG and 2.25% to 15.33% in GG) compared to Inv. networks (mostly 0% in RNG and below 1.17% in GG) and Uni. networks (0% in RNG and 0.79% in GG) as values with upper-triangles (Δ). According to percolation theory [37], a 2D square lattice network maintains its connectivity until the fraction 0.4073 (percolation threshold $pc = 0.5927$) of randomly removed nodes. This critical fraction 0.4073 is larger than the analytical values 0.205 in RNG and 0.365 in GG shown in Table 3. The presence of these grid-like parts increases the critical fraction than the above values in RNG and GG on free node's locations at random.

4 Conclusion

Our study investigates the impact of local community structure on the vulnerability of spatial networks with concentration of nodes. The node's locations are according to the order of real population (Pop.), inverse real population (Inv.), and uniformly at random (Uni.), while the links between nodes are short by using proximity graphs of RNG and GG as modeling road and communication systems, respectively. Remember that Pop., Inv., and Uni. are considered to investigate the effect of strengths of community structure on the robustness. We observed the emergence of local communities in Pop. and Inv. networks connected by short links (see Figs. 3 and 4), which weakens the networks by removing small number of inter-community bridge links (see Figs. 5 and 6). In the details, for the measures of robustness index R and critical fraction q_c , Pop. and Inv. networks are weaker than Uni. networks against intentional attacks and random failures in both RNG and GG, because Pop. and Inv. networks have stronger local communities than Uni. networks (see Figs. 8 and 9). In particular, both R and

q_c decrease with increasing modularity Q (see [S13 Fig.](#), [S14 Fig.](#) and [Fig. 7](#)). Therefore, we conclude that the emergence of local communities weakens the robustness of connectivity in spatial networks.

For this negative impact of local communities on the robustness, it is important to understand how to reduce their effects. Local communities emerge from the spatial concentration of nodes connected by short links. While the strength of local communities could be mitigated by either distributing nodes more evenly or creating long links, the former approach may be impractical due to high land acquisition costs. Therefore, strategically establishing long links offers a more feasible solution to balance reliability and construction costs.

However, our study has several limitations. For example, while we focus on road and communication networks, the applicability of our findings remains to other infrastructure networks, such as power grids and water supply systems. Moreover, although we thoroughly investigated the effects of RB, ID, and RF attacks, the results of other more distractive attacks, such as belief propagation attacks [\[38\]](#) and collective influence attacks [\[39\]](#), on the vulnerability of spatial networks warrants further investigation. In addition, the universal applicability of our conclusions to regions outside Japan requires additional verification through studies in other countries and regions.

List of Abbreviations

RGB Red-Green-Blue (color scheme)

CYM Cyan-Yellow-Magenta (color scheme)

GG Gabriel Graph

RNG Relative Neighborhood Graph

2DL Two-Dimensional Square Lattice

Pop. Population

Inv. Inverse Population

Uni. Uniform

RB Recalculated Betweenness (attack strategy)

ID Initial Degree (attack strategy)

RF Random Failures

SF Scale-Free

ER Erdős-Rényi

SPP Spatial Point Process

LCC Largest Connected Component

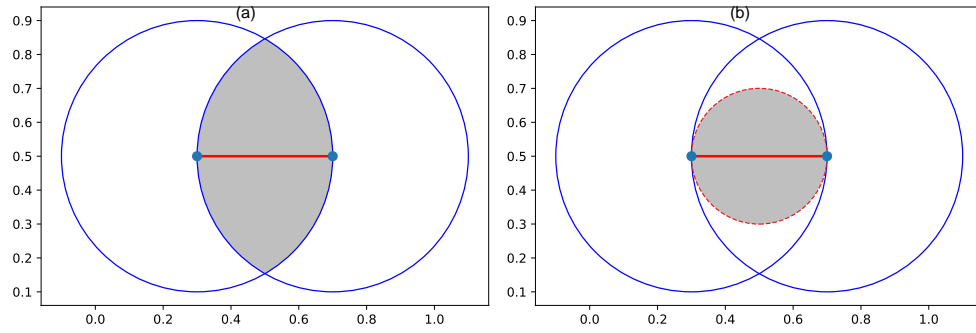


Fig. 1 Illustration of connection constraints for (a) RNG and (b) GG. A link colored by red is established between two nodes colored by blue, when no other node exists within the shaded area.

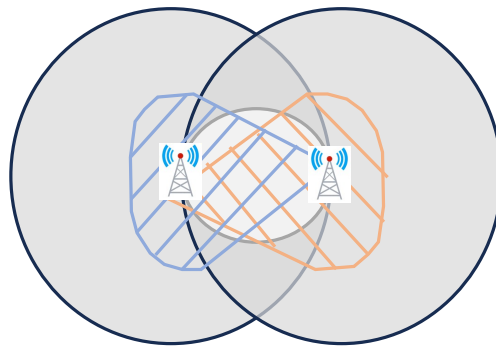


Fig. 2 Coverage diagram of radio waves between two base stations in wireless communication. The ranges of strong beams are shown by blue and orange shades. The center circle represents the signal interference area. If other base stations exist within it, the two stations cannot be connected.

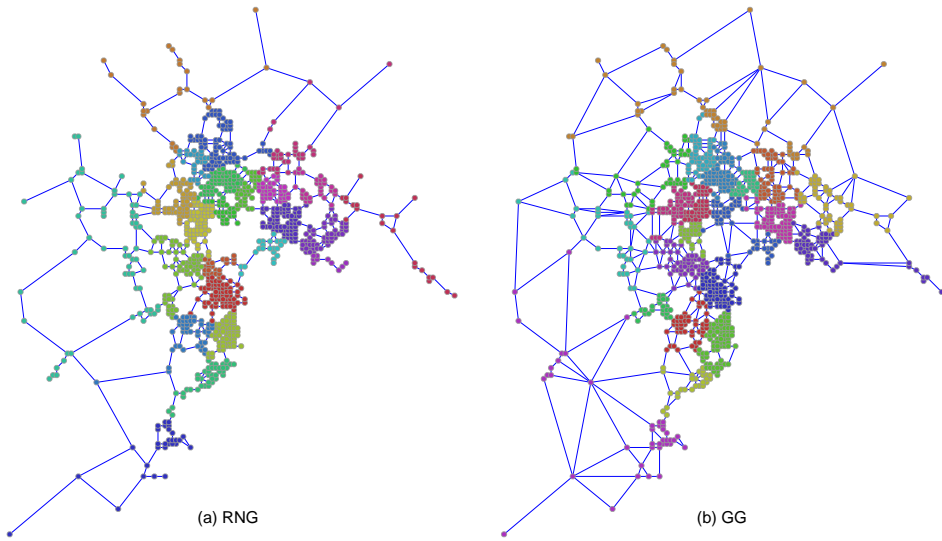


Fig. 3 Visualization of community structure in Tokyo before node removal. $N = 1024$ nodes are located by the decreasing order of population (Pop.). Different colors represent different communities estimated by Louvain method. There are clear community formations particularly in densely populated areas.

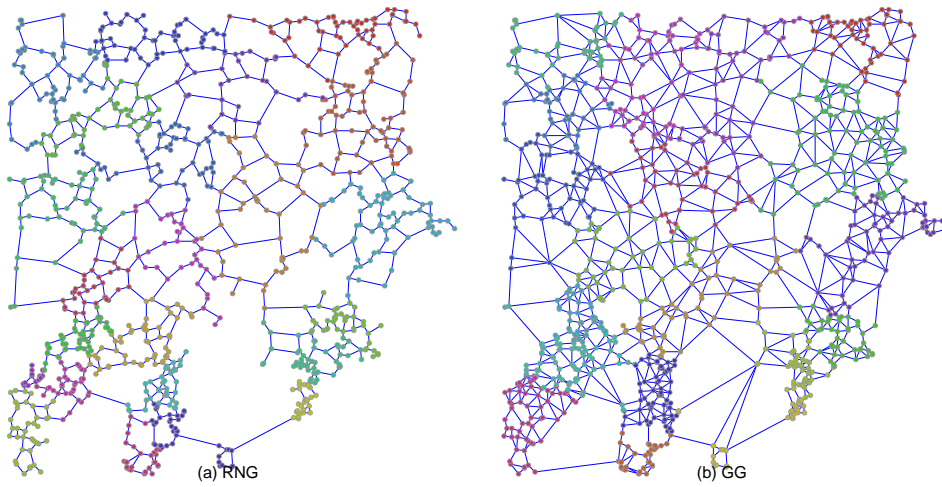


Fig. 4 Visualization of community structure in Tokyo before node removal. $N = 1024$ nodes are located by the inverse order of population (Inv.). Different colors represent different communities estimated by Louvain method. There are different community formations compared to Figure 3.

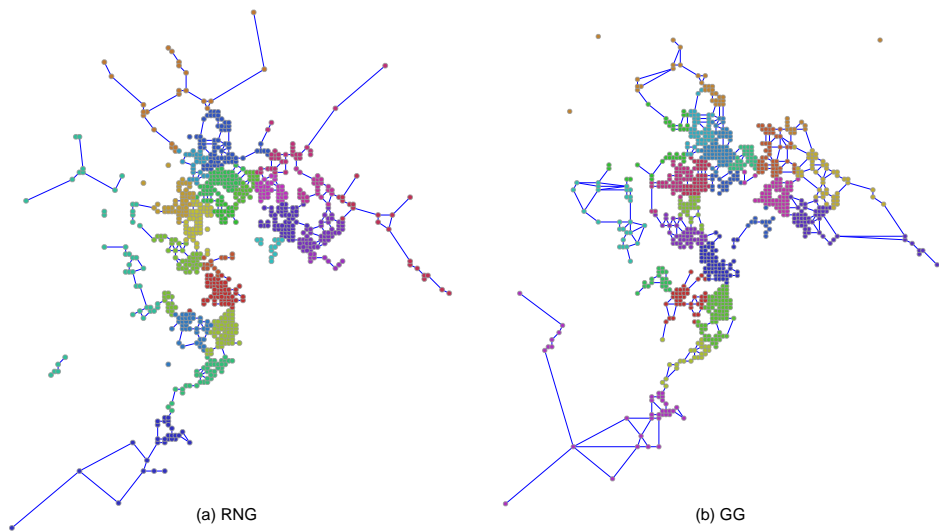


Fig. 5 Tokyo networks with $N = 1024$ nodes after 10% node removals by recalculated betweenness (RB) attacks. The locations of nodes are selected by decreasing order of population (Pop.). The fragmentation is observed by removing links between communities especially in densely populated areas

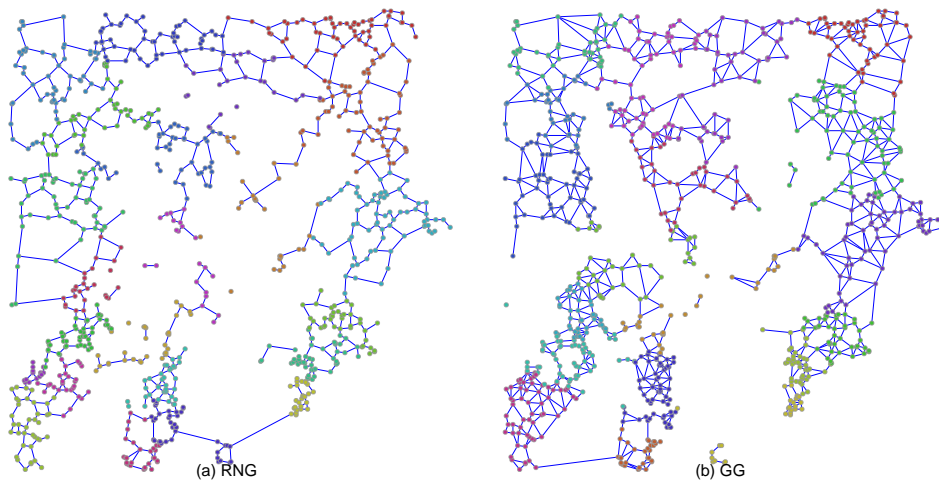


Fig. 6 Tokyo networks with $N = 1024$ nodes after 10% node removals by recalculated betweenness (RB) attacks. The locations of nodes are selected by inverse order of population (Inv.). The fragmentation is observed by removing links between communities which are different as compared to Figure 5.

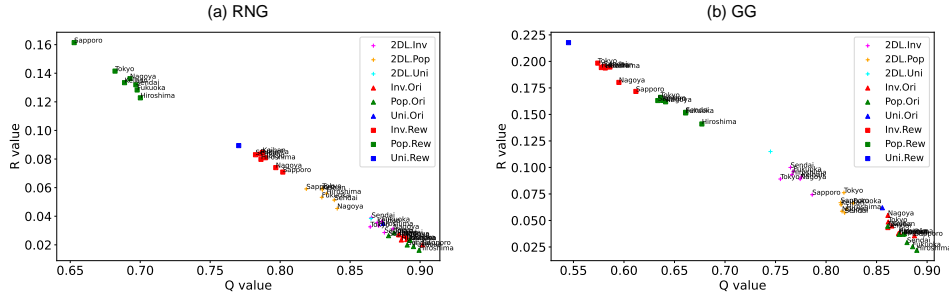


Fig. 7 Relation between robustness index R^{RB} and modularity Q in networks with $N = 1024$ nodes

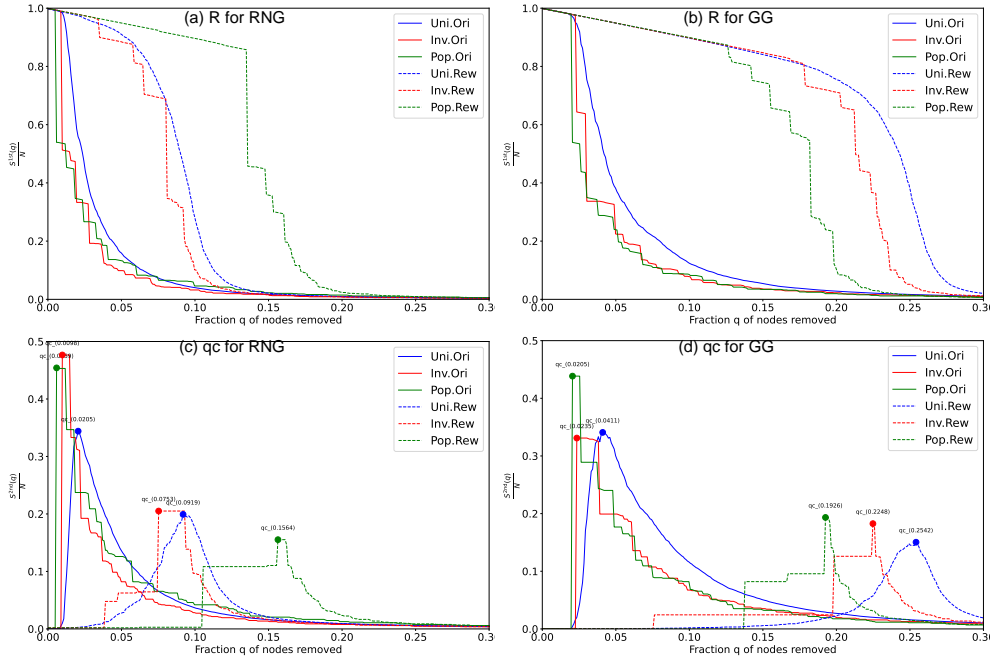


Fig. 8 Robustness against recalculated betweenness (RB) attacks for Tokyo networks with $N = 1024$ nodes. For rewired (Randomized networks) lines, the rewiring process preserves the original degree distributions. Two measures are applied: (a) (b) the relative size $S^{1st}(q)/N$ of largest connected component, and (c) (d) the critical fraction q_c at the peak of the relative size $S^{2nd}(q)/N$ of second largest component.

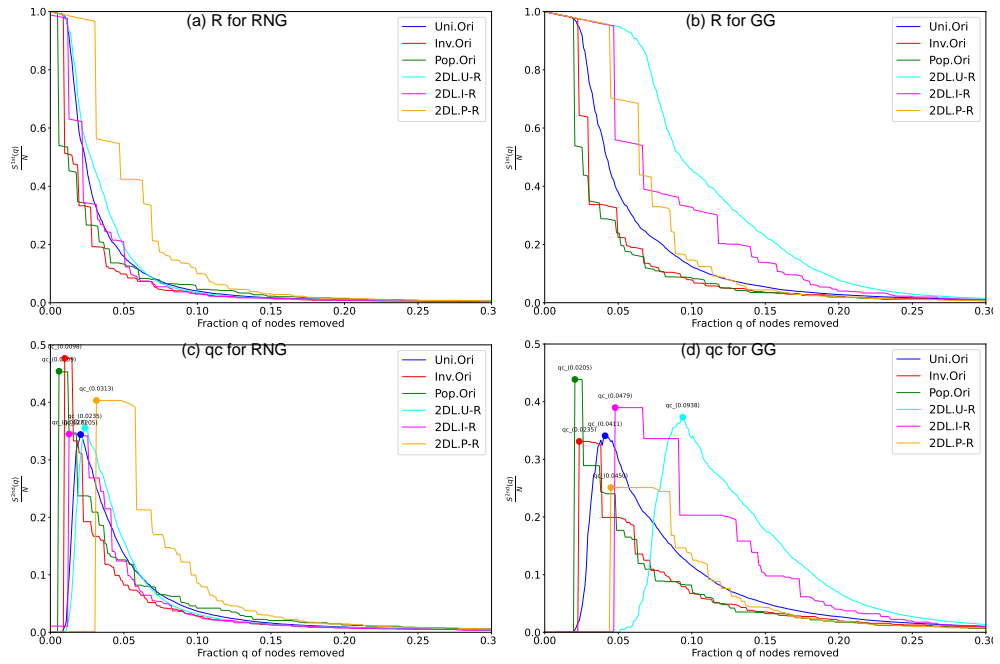


Fig. 9 Robustness against recalculated betweenness (RB) attacks for Tokyo networks with $N = 1024$ nodes. For 2DL (relocated networks) lines, the rewiring process preserves the original degree distributions. Two measures are applied: (a) (b) the relative size $S^{1st}(q)/N$ of largest connected component, and (c) (d) the critical fraction q_c at the peak of the relative size $S^{2nd}(q)/N$ of second largest component.

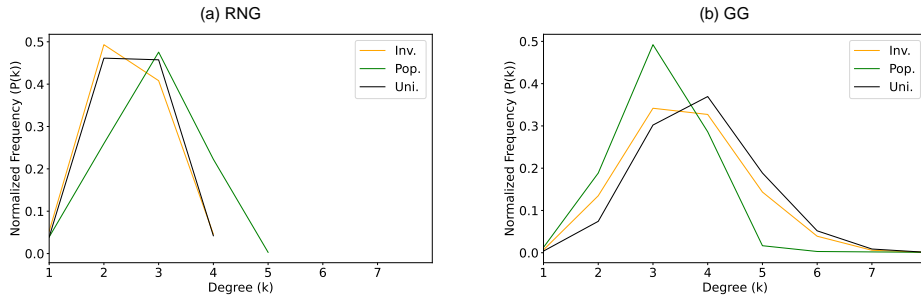


Fig. 10 Similar degree distributions of bell-shapes for Pop., Inv., and Uni. in Tokyo networks with $N = 1024$ nodes.

Cities	Original			Randomized			Relocated			
	RNG Inv.	RNG Pop.	GG Inv. Pop.	RNG Inv.	RNG Pop.	GG Inv. Pop.	RNG Inv.	RNG Pop.	GG Inv. Pop.	
Fukuoka	0.8905 Δ	0.8953 Δ	0.8728 Δ	0.786 Δ	0.6978	0.5776 Δ	0.8726 Δ	0.8298	0.7677 Δ	0.8269 Δ
Hiroshima	0.8866 Δ	0.8993 Δ	0.8717 Δ	0.7863 Δ	0.7001	0.5815 Δ	0.8704 Δ	0.8332	0.7662 Δ	0.8203 Δ
Keihan	0.8903 Δ	0.8924 Δ	0.8651 Δ	0.7874 Δ	0.6888	0.5861 Δ	0.8693 Δ	0.8302	0.7756 Δ	0.8149 Δ
Nagoya	0.8880 Δ	0.8929 Δ	0.8612 Δ	0.7969 Δ	0.6927	0.595 Δ	0.8807 Δ	0.8408	0.7744 Δ	0.8158 Δ
Tokyo	0.8846 Δ	0.8814 Δ	0.8615 Δ	0.7895 Δ	0.682	0.5741 Δ	0.8644	0.8301	0.7548 Δ	0.8177 Δ
Sendai	0.8853 Δ	0.8908 Δ	0.8612 Δ	0.7824 Δ	0.6969	0.58 Δ	0.8653 Δ	0.8387	0.7648 Δ	0.8184 Δ
Sapporo	0.9017 Δ	0.8775 Δ	0.8875 Δ	0.8019 Δ	0.6528	0.6118 Δ	0.8745 Δ	0.8187	0.7863 Δ	0.8144 Δ
Uniform	0.8735		0.8557	0.7704		0.5451	0.8649		0.745	

Table 1 Modularity Q in networks with 1024 nodes for seven major Japanese areas under three different conditions: original networks, after randomization (rewired), and after nodes relocation on a 2DL (relocated). Higher values indicate stronger community structure. Values with upper-triangles (Δ) indicate where the cases of Pop. and Inv. have higher modularity than the case of Uni., while values in bold indicate lower modularity than the case of Uni. for both RNG and GG.

Cities	R^{ID}				q_c^{ID}			
	RNG		GG		RNG		GG	
	Inv.	Pop.	Inv.	Pop.	Inv.	Pop.	Inv.	Pop.
Fukuoka	0.1264	0.2541 Δ	0.2171	0.2693 Δ	0.0901	0.2172 Δ	0.1832	0.2202
Hiroshima	0.1162	0.1319 Δ	0.2332	0.1606	0.0821	0.0981	0.2032	0.1051
Keihan	0.1531 Δ	0.1765 Δ	0.1998	0.1758	0.1692 Δ	0.0751	0.1712	0.1782
Nagoya	0.1404 Δ	0.1943 Δ	0.2238	0.2084	0.1552 Δ	0.1772 Δ	0.2392	0.0631
Tokyo	0.1363 Δ	0.2191 Δ	0.2250	0.2083	0.1361 Δ	0.2412 Δ	0.2362	0.1512
Sendai	0.1240	0.1801 Δ	0.2132	0.1257	0.0591	0.1061	0.1882	0.0170
Sapporo	0.1055	0.1646 Δ	0.1890	0.2042	0.0851	0.1441 Δ	0.1301	0.1522
Uniform	0.132		0.247		0.1351		0.2643	
Analytical	-				0.12		0.263	

Table 2 Robustness index (R^{ID}) and Critical fraction (q_c^{ID}) against Initial Degree (ID) attacks in the original networks with $N = 1024$ nodes for seven major Japanese areas. Higher values indicate greater robustness. Values with upper-triangles (Δ) indicate where the cases of Pop. and Inv. have stronger robustness than the case of the Uni. network.

Cities	R^{RF}				q_c^{RF}			
	RNG		GG		RNG		GG	
	Inv.	Pop.	Inv.	Pop.	Inv.	Pop.	Inv.	Pop.
Fukuoka	0.1573	0.1338	0.2820	0.1902	0.1191	0.0911	0.3724 Δ	0.1682
Hiroshima	0.1476	0.1227	0.2627	0.1510	0.1832	0.0320	0.3093	0.0601
Keihan	0.2040 Δ	0.2001 Δ	0.2486	0.2421	0.1522	0.2382 Δ	0.3844 Δ	0.2773
Nagoya	0.1711	0.2060 Δ	0.2752	0.2068	0.1692	0.0881	0.2653	0.3093
Tokyo	0.1721	0.2146 Δ	0.2998	0.2614	0.1031	0.2873 Δ	0.2332	0.2513
Sendai	0.1771	0.1407	0.2650	0.1806	0.1131	0.0330	0.2843	0.0541
Sapporo	0.1253	0.2053 Δ	0.2126	0.2345	0.1391	0.0330	0.2302	0.4014
Uniform	0.1972		0.3083		0.2112		0.3694	
Analytical	-				0.205		0.365	

Table 3 Robustness index (R^{RF}) and Critical fraction (q_c^{RF}) against random failure (RF) in the original networks with $N = 1024$ nodes for seven major Japanese areas. Higher values indicate greater robustness. Values with upper-triangles (Δ) indicate where the cases of Pop. and Inv. have stronger robustness than the case of the Uni. network.

Cities	RNG		GG	
	Inv.	Pop.	Inv.	Pop.
Fukuoka	2.4492	2.8223 \triangle	3.584	2.9844
Hiroshima	2.4414	2.7852 \triangle	3.5996	2.9199
Keihan	2.4395	2.8535 \triangle	3.5469	3.1367
Nagoya	2.3945	2.8535 \triangle	3.4785	3.1367
Tokyo	2.4473	2.8906 \triangle	3.6113	3.1191
Sendai	2.459	2.834 \triangle	3.582	3.0195
Sapporo	2.3789	3.0684 \triangle	3.3105	3.1563
Uniform	2.5017		3.864	

Table 4 Average degree $\langle k \rangle$ in networks with $N = 1024$ nodes for seven major Japanese areas. Values with upper-triangles (\triangle) indicate cases where Pop. and Inv. show higher $\langle k \rangle$ than the case of Uni.

Cities	RNG		GG	
	Inv.	Pop.	Inv.	Pop.
Fukuoka	0	0.0771 \triangle	0.0039	0.0771 \triangle
Hiroshima	0	0.0205 \triangle	0.0078	0.0205 \triangle
Keihan	0	0.0391 \triangle	0.0078	0.0479 \triangle
Nagoya	0	0.0391 \triangle	0.0088 \triangle	0.0479 \triangle
Tokyo	0	0.0205 \triangle	0.0068	0.0225 \triangle
Sendai	0	0.0459 \triangle	0.0117 \triangle	0.0498 \triangle
Sapporo	0	0.1514 \triangle	0.001	0.1533 \triangle
Uniform	0		0.0079	
Lattice	0.7656			

Table 5 Proportion of grid-like parts in networks with $N = 1024$ nodes for seven major Japanese areas. A grid-like structure is identified when a node has degree 4 with the neighbors of degree 4. Values with upper-triangles (\triangle) indicate cases where the ratio is higher than that of Uni. networks. Note that 2D lattice shows the highest ratio (76.56%) because of its completely ordered grid arrangement.

References

- [1] Newman, M.E.: Modularity and community structure in networks. Proceedings of the National Academy of Sciences in USA **103**(23), 8577–8582 (2006) <https://doi.org/10.1073/pnas.0601602103>
- [2] Girvan, M., Newman, M.E.: Community structure in social and biological networks. Proceedings of the National Academy of Sciences in USA **99**(12), 7821–7826 (2002) <https://doi.org/10.1073/pnas.122653799>
- [3] Gastner, M., Newman, M.: The spatial structure of networks. The European Physical Journal B **2**(49), 247–252 (2006) <https://doi.org/10.1140/epjb/e2006-00046-8>
- [4] Guimera, R., Mossa, S., Turtschi, A., Amaral, L.N.: The worldwide air transportation network: Anomalous centrality, community structure, and cities’ global roles. Proceedings of the National Academy of Sciences **102**(22), 7794–7799 (2005) <https://doi.org/10.1073/pnas.0407994102>
- [5] Kaluza, P., Kölzsch, A., Gastner, M.T., Blasius, B.: The complex network of global cargo ship movements. Journal of the Royal Society Interface **7**(48), 1093–1103 (2010) <https://doi.org/10.1098/rsif.2009.0495>
- [6] Wan, Y., Tan, X., Shu, H.: Finding and evaluating community structures in spatial networks. ISPRS International Journal of Geo-Information **12**(187), 1–20 (2023) <https://doi.org/10.3390/ijgi12050187>
- [7] Cherifi, H., Palla, G., Szymanski, B.K., Lu, X.: On community structure in complex networks: challenges and opportunities. Applied Network Science **4**(1), 117 (2019) <https://doi.org/10.1007/s41109-019-0238-9>

- [8] Li, J., Lai, S., Shuai, Z., Tan, Y., Jia, Y., Yu, M., Song, Z., Peng, X., Xu, Z., Ni, Y., Qiu, H., Yang, J., Liu, Y., Lu, Y.: A comprehensive review of community detection in graphs. *Neurocomputing* **600**, 128169 (2024) <https://doi.org/10.1016/j.neucom.2024.128169>
- [9] Albert, R., Jeong, H., Barabási, A.-L.: Error and attack tolerance of complex networks. *Nature* **406**(6794), 378–382 (2000) <https://doi.org/10.1038/35019019>
- [10] Shai, S., Kenett, D.Y., Kenett, Y.N., Faust, M., Dobson, S., Havlin, S.: Critical tipping point distinguishing two types of transitions in modular network structures. *Physical Review E* **92**(6), 062805 (2015) <https://doi.org/10.1103/PhysRevE.92.062805>
- [11] Nguyen, Q., Vu, T.V., Dinh, H.-D., Cassi, D., Scotognella, F., Alfieri, R., Bellingeri, M.: Modularity affects the robustness of scale-free model and real-world social networks under betweenness and degree-based node attack. *Applied Network Science* **6**, 1–21 (2021) <https://doi.org/10.1007/s41109-021-00426-y>
- [12] Boeing, G.: Urban spatial order: Street network orientation, configuration, and entropy. *Applied Network Science* **4**(1), 1–19 (2019) <https://doi.org/10.1007/s41109-019-0189-1>
- [13] Boccaletti, S., Latora, V., Moreno, Y., Chavez, M., Hwang, D.-U.: Complex networks: Structure and dynamics. *Physics Reports* **424**(4-5), 175–308 (2006) <https://doi.org/10.1016/j.physrep.2005.10.009>
- [14] Hayashi, Y., Matsukubo, J.: Improvement of the robustness on geographical networks by adding shortcuts. *Physica A: Statistical Mechanics and its Applications* **380**, 552–562 (2007) <https://doi.org/10.1016/j.physa.2007.02.080>

- [15] Toussaint, G.T.: The relative neighbourhood graph of a finite planar set. *Pattern Recognition* **12**(4), 261–268 (1980) [https://doi.org/10.1016/0031-3203\(80\)90066-7](https://doi.org/10.1016/0031-3203(80)90066-7)
- [16] Gabriel, K.R., Sokal, R.R.: A new statistical approach to geographic variation analysis. *Systematic Zoology* **18**(3), 259–278 (1969) <https://doi.org/10.2307/2412323>
- [17] Barthelemy, M.: *Spatial Networks: A Complete Introduction: From Graph Theory and Statistical Physics to Real-World Applications*, pp. 319–326. Springer, Cham (2022). Chap. 16. <https://doi.org/10.1007/978-3-030-94106-2>
- [18] Adamatzky, A., Adamatzky, A.: *Bioevaluation of World Transport Networks*, pp. 13–17. World Scientific Publishing Co., Inc., USA (2012). <https://doi.org/10.1142/8482>
- [19] Holme, P., Kim, B.J., Yoon, C.N., Han, S.K.: Attack vulnerability of complex networks. *Physical Review E* **65**(5), 056109 (2002) <https://doi.org/10.1103/PhysRevE.65.056109>
- [20] Barabási, A.-L., Albert, R.: Emergence of scaling in random networks. *Science* **286**(5439), 509–512 (1999) <https://doi.org/10.1126/science.286.5439.509>
- [21] Watanabe, D.: A study on analyzing road network patterns using proximity graphs. *Journal of the City Planning Institute of Japan* **40.3**, 133–138 (2005) <https://doi.org/10.11361/journalcpij.40.3.133>
- [22] Watanabe, D.: A study on analyzing the grid road network patterns using relative neighborhood graph. In: *The Ninth International Symposium on Operations Research and Its Applications*, pp. 112–119 (2010). *Lecture Notes in Operations Research*. Beijing, China: World Publishing ...

- [23] Bose, P., Morin, P., Stojmenović, I., Urrutia, J.: Routing with guaranteed delivery in ad hoc wireless networks. In: Proceedings of the 3rd International Workshop on Discrete Algorithms and Methods for Mobile Computing and Communications. DIALM '99, pp. 48–55. Association for Computing Machinery, New York, NY, USA (1999). <https://doi.org/10.1145/313239.313282> . <https://doi.org/10.1145/313239.313282>
- [24] Karp, B., Kung, H.T.: Gpsr: greedy perimeter stateless routing for wireless networks. In: Proceedings of the 6th Annual International Conference on Mobile Computing and Networking. MobiCom '00, pp. 243–254. Association for Computing Machinery, New York, NY, USA (2000). <https://doi.org/10.1145/345910.345953> . <https://doi.org/10.1145/345910.345953>
- [25] Anderson, E., Phillips, C., Sicker, D., Grunwald, D.: Modeling environmental effects on directionality in wireless networks. In: 2009 7th International Symposium on Modeling and Optimization in Mobile, Ad Hoc, and Wireless Networks, pp. 1–7 (2009). <https://doi.org/10.1109/WIOPT.2009.5291577>
- [26] Singh, J., Kaur, G., Kaur, G.: Determining best setup sites for cellular towers using fuzzy logic. In: 2015 International Conference on Futuristic Trends on Computational Analysis and Knowledge Management (ABLAZE), pp. 256–260 (2015). <https://doi.org/10.1109/ABLAZE.2015.7155002> . IEEE
- [27] Onim, A., Kihato, P., Musyoki, S.: Optimization of base station location in 3g networks using fuzzy clustering and mesh adaptive direct search. In: Proceedings of Sustainable Research and Innovation Conference, pp. 30–35 (2014)
- [28] Office for National Statistics: Population density, Census 2021. [Online; accessed 01-August-2024] (2021). <https://www.ons.gov.uk/census/maps/choropleth/population/population-density/population-density/>

persons-per-square-kilometre

- [29] Keeler, H.P.: Notes on the poisson point process. Weierstrass Inst., Berlin, Germany, Technical Report (2016)
- [30] Kittel, C., McEuen, P.: Introduction to Solid State Physics, 8th edn. John Wiley & Sons, Hoboken, NJ (2018)
- [31] Statistics Bureau of Japan: 2010 Census of Japan. <https://www.stat.go.jp/english/data/kokusei/2010/summary.html>. [Online; accessed 2024-08-05] (2010)
- [32] Newman, M.E.J., Girvan, M.: Finding and evaluating community structure in networks. *Physical Review E* **69**(2), 026113 (2004) <https://doi.org/10.1103/PhysRevE.69.026113>
- [33] Blondel, V.D., Guillaume, J.-L., Lambiotte, R., Lefebvre, E.: Fast unfolding of communities in large networks. *Journal of Statistical Mechanics: Theory and Experiment* **2008**(10), 10008 (2008) <https://doi.org/10.1088/1742-5468/2008/10/P10008>
- [34] Schneider, C.M., Moreira, A.A., Andrade Jr, J.S., Havlin, S., Herrmann, H.J.: Mitigation of malicious attacks on networks. *Proceedings of the National Academy of Sciences in USA* **108**(10), 3838–3841 (2011) <https://doi.org/10.1073/pnas.1009440108>
- [35] Callaway, D.S., Newman, M.E., Strogatz, S.H., Watts, D.J.: Network robustness and fragility: Percolation on random graphs. *Physical Review Letters* **85**(25), 5468 (2000) <https://doi.org/10.1103/PhysRevLett.85.5468>
- [36] Norrenbrock, C., Melchert, O., Hartmann, A.K.: Fragmentation properties of two-dimensional proximity graphs considering random failures and targeted attacks.

Physical Review E **94**(6), 062125 (2016) <https://doi.org/10.1103/PhysRevE.94.062125>

[37] Stauffer, D., Aharony, A.: Introduction To Percolation Theory: Second Edition, 2nd edn., p. 192. Taylor & Francis, London (1992). <https://doi.org/10.1201/9781315274386>

[38] Mugisha, S., Zhou, H.-J.: Identifying optimal targets of network attack by belief propagation. Phys. Rev. E **94**, 012305 (2016) <https://doi.org/10.1103/PhysRevE.94.012305>

[39] Morone, F., Makse, H.: Influence maximization in complex networks through optimal percolation. Nature **524**, 65–68 (2015) <https://doi.org/10.1038/nature14604>

Availability of data and materials

The population data used in this study are available from the “Regional Mesh Statistics: First Regional Division, 2010 Population Census (World Geodetic System)” provided by the Statistical Information Institute for Consulting and Analysis (SINFONICA). The data were purchased under license from SINFONICA (located at Nogaku Shorin Building 5F, 3-6 Kanda-Jinbocho, Chiyoda-ku, Tokyo 101-0051, Japan). These data are subject to usage restrictions. Researchers interested in accessing these data should contact SINFONICA (<https://www.sinfonica.or.jp/>) for purchase and licensing information.

The code used to generate the results is also available from the corresponding author upon reasonable request.

Competing interests

The authors declare that they have no competing interests.

Funding

JSPS KAKENHI Grant Number JP.21H03425

Authors' contributions

Conceptualization: Yukio Hayashi.

Funding acquisition: Yukio Hayashi.

Investigation: Yingzhou Mou, Yukio Hayashi.

Methodology: Yingzhou Mou, Yukio Hayashi.

Supervision: Yukio Hayashi.

Visualization: Yingzhou Mou.

Writing - original draft: Yingzhou Mou.

Writing - review & editing: Yingzhou Mou, Yukio Hayashi.

Acknowledgements

This research is supported in part by JSPS KAKENHI Grant Number JP.21H03425

Authors' information

1. Yingzhou MOU (Corresponding author)

Japan Advanced Institute of Science and Technology, Nomi-city,
Ishikawa 923-1292, Japan

E-mail: mouyingzhou@outlook.com

2. Yukio HAYASHI

Japan Advanced Institute of Science and Technology, Nomi-city,
Ishikawa 923-1292, Japan

E-mail: yhayashi@jaist.ac.jp

Supporting Information

S1 Fig. fukuoka_descend_1024_community_2in1.pdf: Visualization of community structures in Fukuoka before node removal. $N = 1024$ nodes are located by the decreasing order of population (Pop.). Different colors represent different communities estimated by Louvain method. There are clear community formations particularly in densely populated areas.

S2 Fig. fukuoka_ascend_1024_community_2in1.pdf: Visualization of community structures in Fukuoka before node removal. $N = 1024$ nodes are located by the inverse order of population (Inv.). Different colors represent different communities estimated by Louvain method. There are different community formations compared to S1 Fig.

S3 Fig. hirosima_descend_1024_community_2in1.pdf: Visualization of community structures in Hiroshima before node removal. $N = 1024$ nodes are located by the decreasing order of population (Pop.). Different colors represent different communities estimated by Louvain method. There are clear community formations particularly in densely populated areas.

S4 Fig. hirosima_ascend_1024_community_2in1.pdf: Visualization of community structures in Hiroshima before node removal. $N = 1024$ nodes are located by the inverse order of population (Inv.). Different colors represent different communities estimated by Louvain method. There are different community formations compared to S3 Fig.

S5 Fig. keihan_descend_1024_community_2in1.pdf: Visualization of community structures in Keihan before node removal. $N = 1024$ nodes are located by the decreasing order of population (Pop.). Different colors represent different communities estimated by Louvain method. There are clear community formations particularly in densely populated areas.

S6 Fig. keihan_ascend_1024_community_2in1.pdf: Visualization of community structures in Keihan before node removal. $N = 1024$ nodes are located by the inverse

order of population (Inv.). Different colors represent different communities estimated by Louvain method. There are different community formations compared to S5 Fig.

S7 Fig. nagoya_descend_1024_community_2in1.pdf: Visualization of community structures in Nagoya before node removal. $N = 1024$ nodes are located by the decreasing order of population (Pop.). Different colors represent different communities estimated by Louvain method. There are clear community formations particularly in densely populated areas.

S8 Fig. nagoya_ascend_1024_community_2in1.pdf: Visualization of community structures in Nagoya before node removal. $N = 1024$ nodes are located by the inverse order of population (Inv.). Different colors represent different communities estimated by Louvain method. There are different community formations compared to S7 Fig.

S9 Fig. sendai_descend_1024_community_2in1.pdf: Visualization of community structures in Sendai before node removal. $N = 1024$ nodes are located by the decreasing order of population (Pop.). Different colors represent different communities estimated by Louvain method. There are clear community formations particularly in densely populated areas.

S10 Fig. sendai_ascend_1024_community_2in1.pdf: Visualization of community structures in Sendai before node removal. $N = 1024$ nodes are located by the inverse order of population (Inv.). Different colors represent different communities estimated by Louvain method. There are different community formations compared to S9 Fig.

S11 Fig. sapporo_descend_1024_community_2in1.pdf: Visualization of community structures in Sapporo before node removal. $N = 1024$ nodes are located by the decreasing order of population (Pop.). Different colors represent different communities estimated by Louvain method. There are clear community formations particularly in densely populated areas.

S12 Fig. sapporo_ascend_1024_community_2in1.pdf: Visualization of community structures in Sapporo before node removal. $N = 1024$ nodes are located by the

inverse order of population (Inv.). Different colors represent different communities estimated by Louvain method. There are different community formations compared to S11 Fig.

S13 Fig. tokyo_rng_qrhc_3in1.pdf: Increasing modularity Q vs. decreasing robustness index R^{RB} or critical fraction q_c^{PRB} for varying the size N in Tokyo RNG networks.

S14 Fig. tokyo_gg_qrhc_3in1.pdf: Increasing modularity Q vs. decreasing robustness index R^{RB} or critical fraction q_c^{PRB} for varying the size N in Tokyo GG networks.

S15 Fig. tokyo_1024_rnqc2grid_2in1.pdf: Scatter plots show relation between network robustness measures (a for R and b for q_c) and the proportion of grid-like parts against random failures (RF). Networks with $N = 1024$ nodes are considered, where Pop. networks (green) show notably higher proportions of grid-like parts compared to Inv. (red) and Uni. (blue) networks. See the text at the end of subsection 3.3 for the detail.

S16 Fig. Fukuoka_100_3combined_4in1.pdf: Robustness against recalculated betweenness (RB) attacks for Fukuoka networks with $N = 100$ nodes. For both Rew (Randomized networks) and 2DL lines, the rewiring process preserves the original degree distributions. Two measures are applied: (a) (b) $S^{1st}(q)/N$ the relative size of largest connected component, and (c) (d) $S^{2nd}(q)/N$ the critical fraction q_c at the peak of the relative size of second largest component.

S17 Fig. Hiroshima_100_3combined_4in1.pdf: Robustness against recalculated betweenness (RB) attacks for Hiroshima networks with $N = 100$ nodes. For both Rew (Randomized networks) and 2DL lines, the rewiring process preserves the original degree distributions. Two measures are applied: (a) (b) $S^{1st}(q)/N$ the relative size of largest connected component, and (c) (d) $S^{2nd}(q)/N$ the critical fraction q_c at the peak of the relative size of second largest component.

S18 Fig. Keihan_100_3combined_4in1.pdf: Robustness against recalculated betweenness (RB) attacks for Keihan networks with $N = 100$ nodes. For both Rew (Randomized networks) and 2DL lines, the rewiring process preserves the original degree distributions. Two measures are applied: (a) (b) $S^{1st}(q)/N$ the relative size of largest connected component, and (c) (d) $S^{2nd}(q)/N$ the critical fraction q_c at the peak of the relative size of second largest component.

S19 Fig. Nagoya_100_3combined_4in1.pdf: Robustness against recalculated betweenness (RB) attacks for Nagoya networks with $N = 100$ nodes. For both Rew (Randomized networks) and 2DL lines, the rewiring process preserves the original degree distributions. Two measures are applied: (a) (b) $S^{1st}(q)/N$ the relative size of largest connected component, and (c) (d) $S^{2nd}(q)/N$ the critical fraction q_c at the peak of the relative size of second largest component.

S20 Fig. Tokyo_100_3combined_4in1.pdf: Robustness against recalculated betweenness (RB) attacks for Tokyo networks with $N = 100$ nodes. For both Rew (Randomized networks) and 2DL lines, the rewiring process preserves the original degree distributions. Two measures are applied: (a) (b) $S^{1st}(q)/N$ the relative size of largest connected component, and (c) (d) $S^{2nd}(q)/N$ the critical fraction q_c at the peak of the relative size of second largest component.

S21 Fig. Sendai_100_3combined_4in1.pdf: Robustness against recalculated betweenness (RB) attacks for Sendai networks with $N = 100$ nodes. For both Rew (Randomized networks) and 2DL lines, the rewiring process preserves the original degree distributions. Two measures are applied: (a) (b) $S^{1st}(q)/N$ the relative size of largest connected component, and (c) (d) $S^{2nd}(q)/N$ the critical fraction q_c at the peak of the relative size of second largest component.

S22 Fig. Sapporo_100_3combined_4in1.pdf: Robustness against recalculated betweenness (RB) attacks for Sapporo networks with $N = 100$ nodes. For both Rew (Randomized networks) and 2DL lines, the rewiring process preserves the original

degree distributions. Two measures are applied: (a) (b) $S^{1st}(q)/N$ the relative size of largest connected component, and (c) (d) $S^{2nd}(q)/N$ the critical fraction q_c at the peak of the relative size of second largest component.

S23 Fig. Fukuoka_1024_3combined_4in1.pdf: Robustness against recalculated betweenness (RB) attacks for Fukuoka networks with $N = 1024$ nodes. For both Rew (Randomized networks) and 2DL lines, the rewiring process preserves the original degree distributions. Two measures are applied: (a) (b) $S^{1st}(q)/N$ the relative size of largest connected component, and (c) (d) $S^{2nd}(q)/N$ the critical fraction q_c at the peak of the relative size of second largest component.

S24 Fig. Hiroshima_1024_3combined_4in1.pdf: Robustness against recalculated betweenness (RB) attacks for Hiroshima networks with $N = 1024$ nodes. For both Rew (Randomized networks) and 2DL lines, the rewiring process preserves the original degree distributions. Two measures are applied: (a) (b) $S^{1st}(q)/N$ the relative size of largest connected component, and (c) (d) $S^{2nd}(q)/N$ the critical fraction q_c at the peak of the relative size of second largest component.

S25 Fig. Keihan_1024_3combined_4in1.pdf: Robustness against recalculated betweenness (RB) attacks for Keihan networks with $N = 1024$ nodes. For both Rew (Randomized networks) and 2DL lines, the rewiring process preserves the original degree distributions. Two measures are applied: (a) (b) $S^{1st}(q)/N$ the relative size of largest connected component, and (c) (d) $S^{2nd}(q)/N$ the critical fraction q_c at the peak of the relative size of second largest component.

S26 Fig. Nagoya_1024_3combined_4in1.pdf: Robustness against recalculated betweenness (RB) attacks for Nagoya networks with $N = 1024$ nodes. For both Rew (Randomized networks) and 2DL lines, the rewiring process preserves the original degree distributions. Two measures are applied: (a) (b) $S^{1st}(q)/N$ the relative size of largest connected component, and (c) (d) $S^{2nd}(q)/N$ the critical fraction q_c at the peak of the relative size of second largest component.

S27 Fig. Sendai_1024_3combined_4in1.pdf: Robustness against recalculated betweenness (RB) attacks for Sendai networks with $N = 1024$ nodes. For both Rew (Randomized networks) and 2DL lines, the rewiring process preserves the original degree distributions. Two measures are applied: (a) (b) $S^{1st}(q)/N$ the relative size of largest connected component, and (c) (d) $S^{2nd}(q)/N$ the critical fraction q_c at the peak of the relative size of second largest component.

S28 Fig. Sapporo_1024_3combined_4in1.pdf: Robustness against recalculated betweenness (RB) attacks for Sapporo networks with $N = 1024$ nodes. For both Rew (Randomized networks) and 2DL lines, the rewiring process preserves the original degree distributions. Two measures are applied: (a) (b) $S^{1st}(q)/N$ the relative size of largest connected component, and (c) (d) $S^{2nd}(q)/N$ the critical fraction q_c at the peak of the relative size of second largest component.

S29 Fig. Fukuoka_10000_3combined_4in1.pdf: Robustness against recalculated betweenness (RB) attacks for Fukuoka networks with $N = 10000$ nodes. For both Rew (Randomized networks) and 2DL lines, the rewiring process preserves the original degree distributions. Two measures are applied: (a) (b) $S^{1st}(q)/N$ the relative size of largest connected component, and (c) (d) $S^{2nd}(q)/N$ the critical fraction q_c at the peak of the relative size of second largest component.

S30 Fig. Hiroshima_10000_3combined_4in1.pdf: Robustness against recalculated betweenness (RB) attacks for Hiroshima networks with $N = 10000$ nodes. For both Rew (Randomized networks) and 2DL lines, the rewiring process preserves the original degree distributions. Two measures are applied: (a) (b) $S^{1st}(q)/N$ the relative size of largest connected component, and (c) (d) $S^{2nd}(q)/N$ the critical fraction q_c at the peak of the relative size of second largest component.

S31 Fig. Keihan_10000_3combined_4in1.pdf: Robustness against recalculated betweenness (RB) attacks for Keihan networks with $N = 10000$ nodes. For both Rew (Randomized networks) and 2DL lines, the rewiring process preserves the original

degree distributions. Two measures are applied: (a) (b) $S^{1st}(q)/N$ the relative size of largest connected component, and (c) (d) $S^{2nd}(q)/N$ the critical fraction q_c at the peak of the relative size of second largest component.

S32 Fig. Nagoya_10000_3combined_4in1.pdf: Robustness against recalculated betweenness (RB) attacks for Nagoya networks with $N = 10000$ nodes. For both Rew (Randomized networks) and 2DL lines, the rewiring process preserves the original degree distributions. Two measures are applied: (a) (b) $S^{1st}(q)/N$ the relative size of largest connected component, and (c) (d) $S^{2nd}(q)/N$ the critical fraction q_c at the peak of the relative size of second largest component.

S33 Fig. Tokyo_10000_3combined_4in1.pdf: Robustness against recalculated betweenness (RB) attacks for Tokyo networks with $N = 10000$ nodes. For both Rew (Randomized networks) and 2DL lines, the rewiring process preserves the original degree distributions. Two measures are applied: (a) (b) $S^{1st}(q)/N$ the relative size of largest connected component, and (c) (d) $S^{2nd}(q)/N$ the critical fraction q_c at the peak of the relative size of second largest component.

S34 Fig. Sendai_10000_3combined_4in1.pdf: Robustness against recalculated betweenness (RB) attacks for Sendai networks with $N = 10000$ nodes. For both Rew (Randomized networks) and 2DL lines, the rewiring process preserves the original degree distributions. Two measures are applied: (a) (b) $S^{1st}(q)/N$ the relative size of largest connected component, and (c) (d) $S^{2nd}(q)/N$ the critical fraction q_c at the peak of the relative size of second largest component.

S35 Fig. Sapporo_10000_3combined_4in1.pdf: Robustness against recalculated betweenness (RB) attacks for Sapporo networks with $N = 10000$ nodes. For both Rew (Randomized networks) and 2DL lines, the rewiring process preserves the original degree distributions. Two measures are applied: (a) (b) $S^{1st}(q)/N$ the relative size of largest connected component, and (c) (d) $S^{2nd}(q)/N$ the critical fraction q_c at the peak of the relative size of second largest component.

S36 Fig. r2q_100_2in1.pdf Relation between robustness index R^{RB} and modularity Q in networks with $N = 100$ nodes.

S37 Fig.r2q_10000_2in1.pdf Relation between robustness index R^{RB} and modularity Q in networks with $N = 10000$ nodes

S1 Table r_qc_rb_100: Robustness index (R^{RB}) and Critical fraction (q_c^{RB}) against Recalculated Betweenness (RB) attacks in networks with $N = 100$ nodes for seven major Japanese areas. Higher values indicate greater robustness of connectivity. For R^{RB} , values with upper-triangles (Δ) indicate higher robustness than Uni. case, while values with lower-triangles (∇) indicate lower robustness than Uni. case. For q_c^{RB} , all values are marked with lower-triangles (∇) as they show lower robustness than Uni. case.

S2 Table r_qc_rb_1024: Robustness index (R^{RB}) and Critical fraction (q_c^{RB}) against Recalculated Betweenness (RB) attacks in networks with $N = 1024$ nodes for seven major Japanese areas. Higher values indicate greater robustness of connectivity. Values with lower-triangles (∇) indicate where the cases of Pop. and Inv. have lower robustness of connectivity than the cases of Uni. for both RNG and GG.

S3 Table r_qc_rb_10000: Robustness index (R^{RB}) and Critical fraction (q_c^{RB}) against Recalculated Betweenness (RB) attacks in networks with $N = 10000$ nodes for seven major Japanese areas. Higher values indicate greater robustness of connectivity. Values with lower-triangles (∇) indicate where the cases of Pop. and Inv. have lower robustness of connectivity than the cases of Uni. for both RNG and GG.

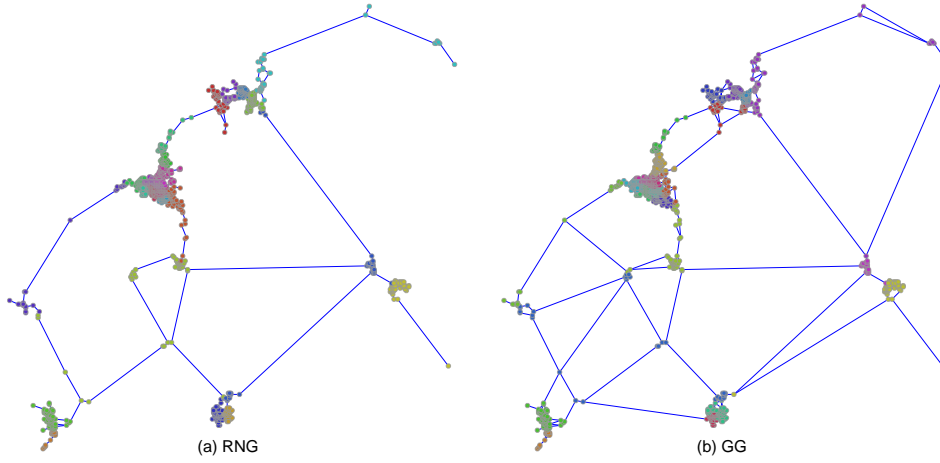
S4 Table average_degree_100: Average degree $\langle k \rangle$ in networks with $(N) = 100$ nodes for seven major Japanese areas. Higher average degrees mean more links per node in the network. Values with upper-triangles (Δ) indicate where the cases of Pop. and Inv. have higher $\langle k \rangle$ than the cases of Uni. for both RNG and GG.

S5 Table average_degree_10000: Average degree $\langle k \rangle$ in networks with $(N) = 10000$ nodes for seven major Japanese areas. Higher average degrees mean more links

per node in the network. Values with upper-triangles (Δ) indicate where the cases of Pop. and Inv. have higher $\langle k \rangle$ than the cases of Uni. for both RNG and GG.

S6 Table q_values_100: Modularity Q in networks with 100 nodes for seven major Japanese areas. Higher values indicate stronger community structures. Values with upper-triangles (Δ) or lower-triangles (∇) indicate where the cases of Pop. and Inv. have higher or lower modularity than the case of Uni. for both RNG and GG. Note the generally higher modularity in Pop. and Inv. compared to Uni. networks for both RNG and GG.

S7 Table q_values_10000: Modularity Q in networks with 10000 nodes for seven major Japanese areas. Higher values indicate stronger community structures. Values with upper-triangles (Δ) indicate where the cases of Pop. and Inv. have higher modularity than the case of Uni. for both RNG and GG. Note the generally higher modularity in Pop. and Inv. compared to Uni. networks for both RNG and GG.



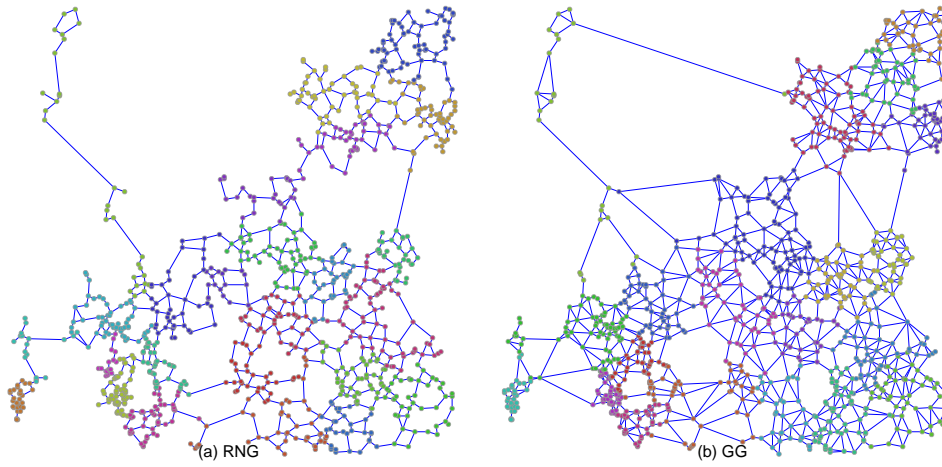
S1 Fig. Visualization of community structures in Fukuoka before node removal. $N = 1024$ nodes are located by the decreasing order of population (Pop.). Different colors represent different communities estimated by Louvain method. There are clear community formations particularly in densely populated areas.

Appendix

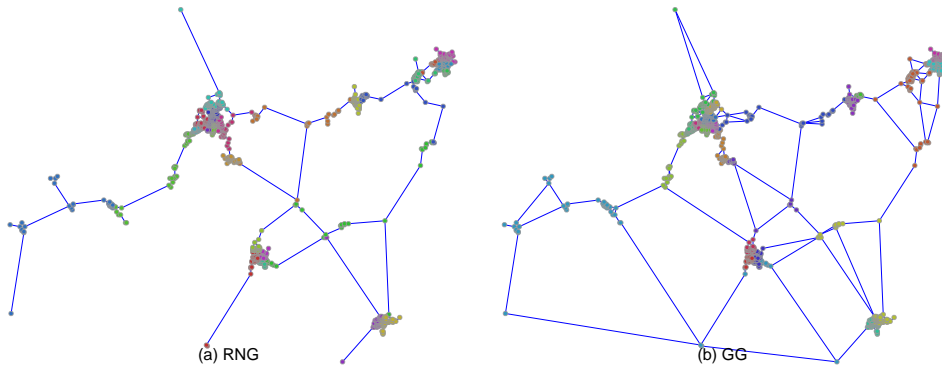
.1 Visualization maps. before attacks

3

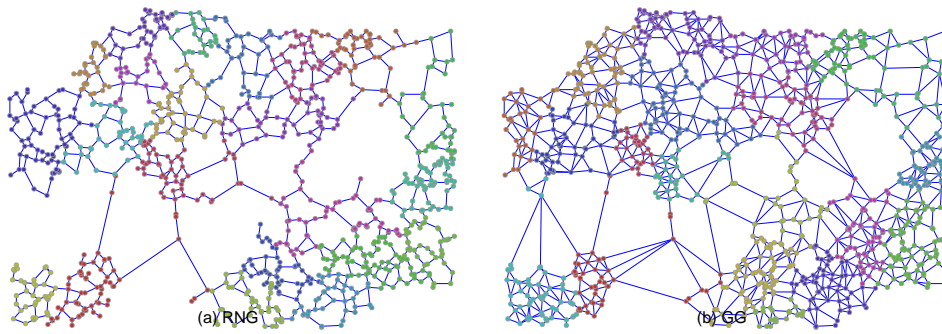
.2 Visualization maps, after 10% node removals



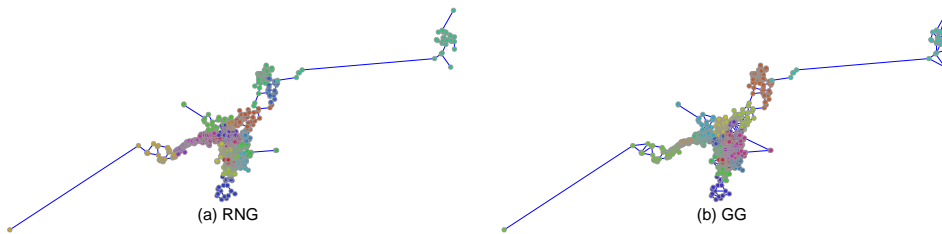
S2 Fig. Visualization of community structures in Fukuoka before node removal. $N = 1024$ nodes are located by the inverse order of population (Inv.). Different colors represent different communities estimated by Louvain method. There are different community formations compared to Figure S1 Fig..



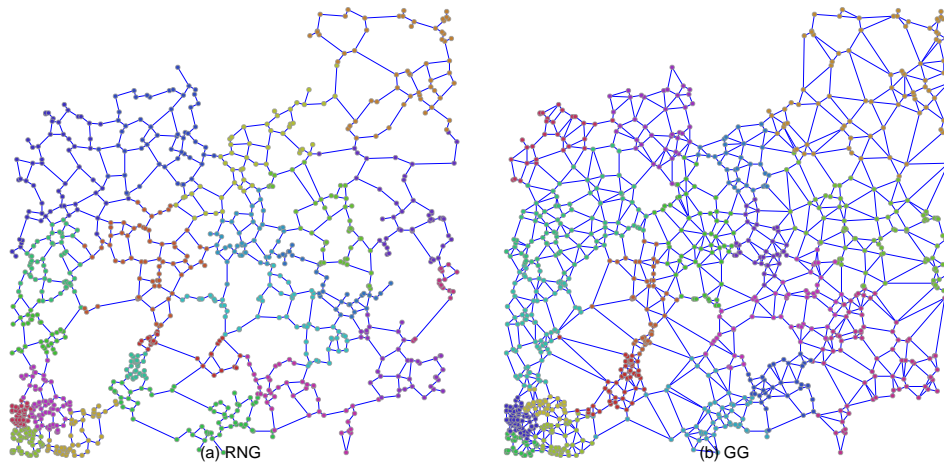
S3 Fig. Visualization of community structures in Hiroshima before node removal. $N = 1024$ nodes are located by the decreasing order of population (Pop.). Different colors represent different communities estimated by Louvain method. There are clear community formations particularly in densely populated areas.



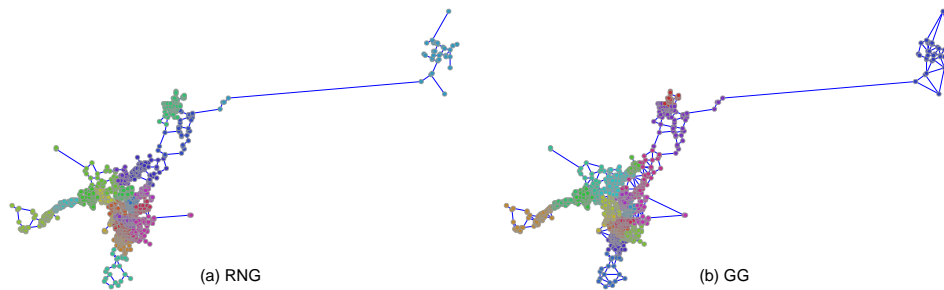
S4 Fig. Visualization of community structures in Hiroshima before node removal. $N = 1024$ nodes are located by the inverse order of population (Inv.). Different colors represent different communities estimated by Louvain method. There are different community formations compared to Figure S3 Fig..



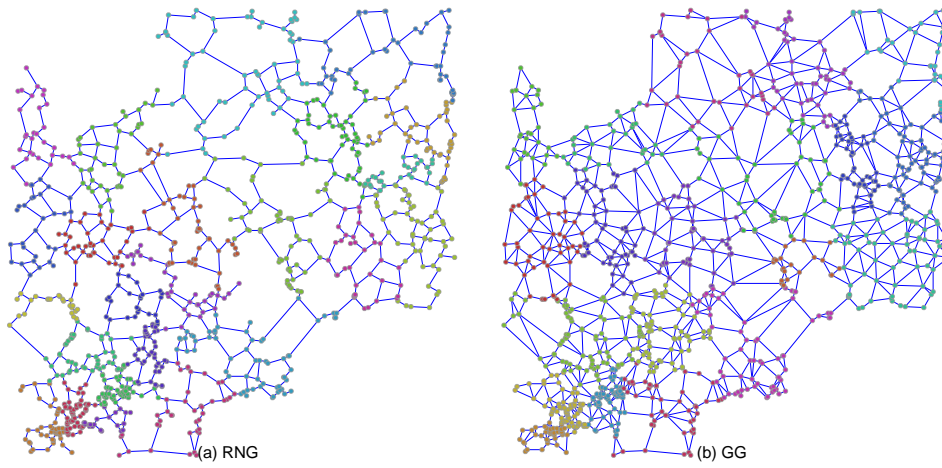
S5 Fig. Visualization of community structures in Keihan before node removal. $N = 1024$ nodes are located by the decreasing order of population (Pop.). Different colors represent different communities estimated by Louvain method. There are clear community formations particularly in densely populated areas.



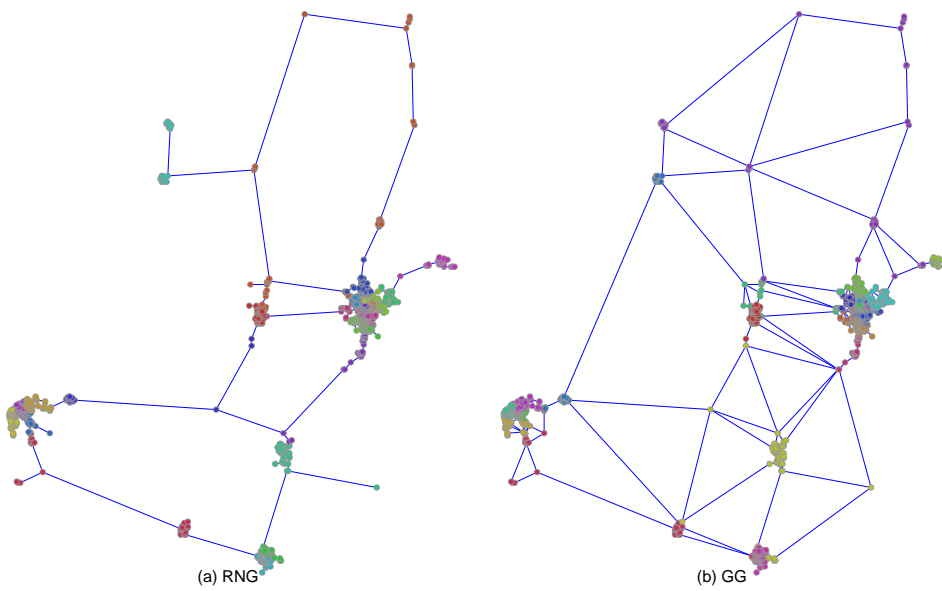
S6 Fig. Visualization of community structures in Keihan before node removal. $N = 1024$ nodes are located by the inverse order of population (Inv.). Different colors represent different communities estimated by Louvain method. There are different community formations compared to Figure S5 Fig..



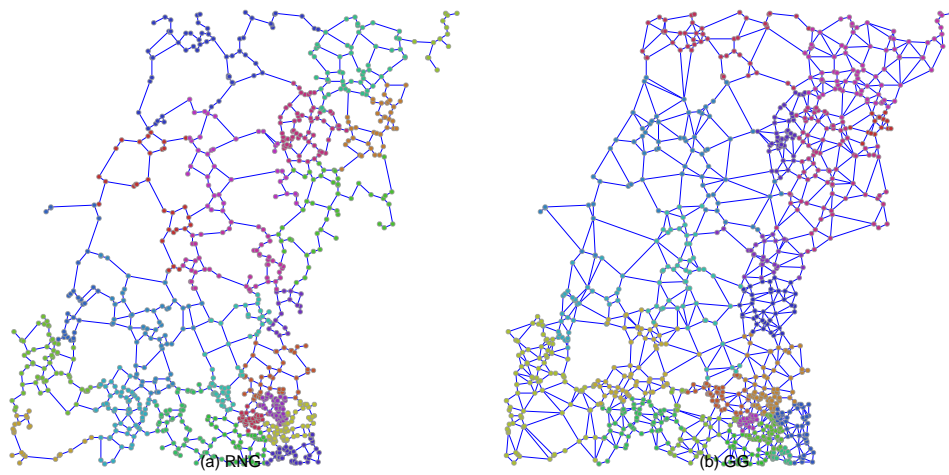
S7 Fig. Visualization of community structures in Nagoya before node removal. $N = 1024$ nodes are located by the decreasing order of population (Pop.). Different colors represent different communities estimated by Louvain method. There are clear community formations particularly in densely populated areas.



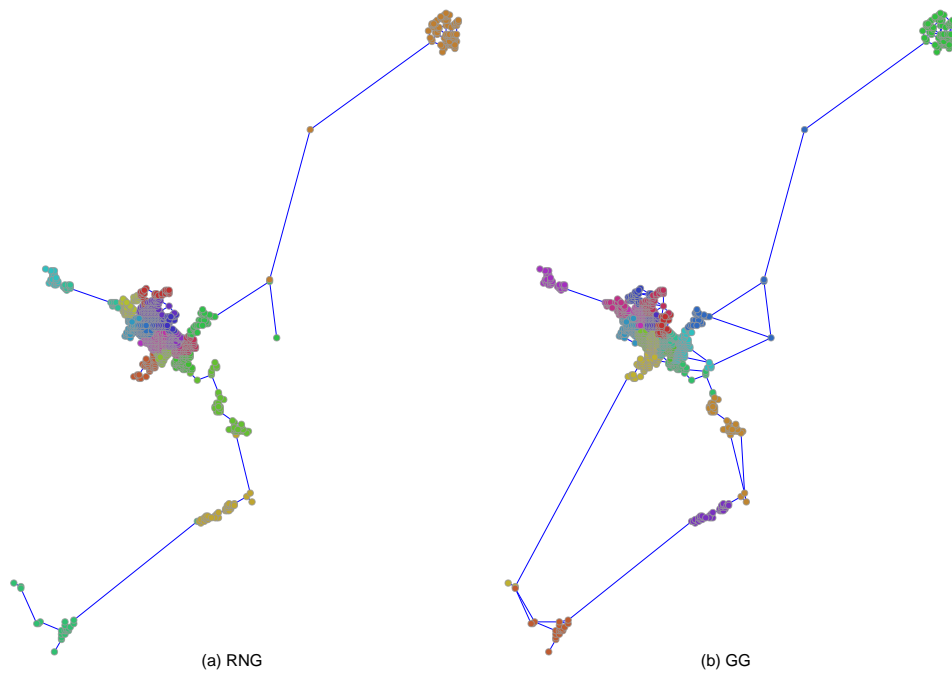
S8 Fig. Visualization of community structures in Nagoya before node removal. $N = 1024$ nodes are located by the inverse order of population (Inv.). Different colors represent different communities estimated by Louvain method. There are different community formations compared to Figure S7 Fig..



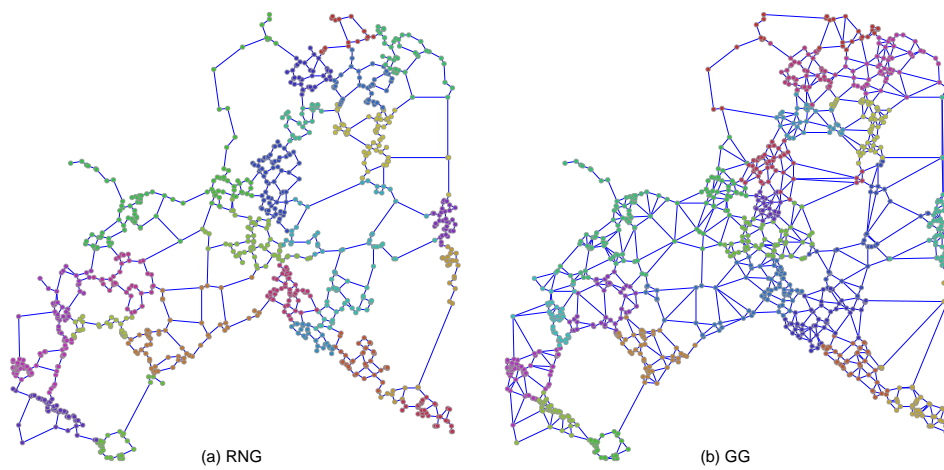
S9 Fig. Visualization of community structures in Sendai before node removal. $N = 1024$ nodes are located by the decreasing order of population (Pop.). Different colors represent different communities estimated by Louvain method. There are clear community formations particularly in densely populated areas.



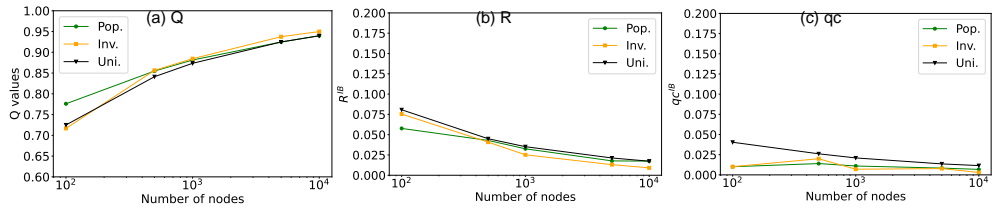
S10 Fig. Visualization of community structures in Sendai before node removal. $N = 1024$ nodes are located by the inverse order of population (Inv.). Different colors represent different communities estimated by Louvain method. There are different community formations compared to Figure S9 Fig..



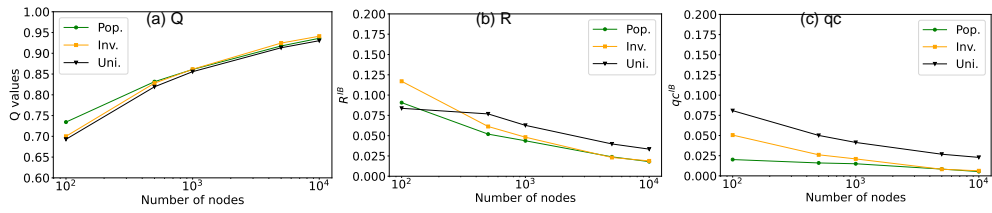
S11 Fig. Visualization of community structures in Sapporo before node removal. $N = 1024$ nodes are located by the decreasing order of population (Pop.). Different colors represent different communities estimated by Louvain method. There are clear community formations particularly in densely populated areas.



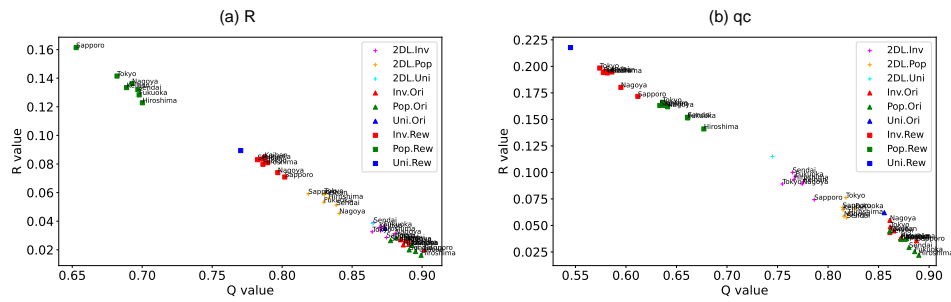
S12 Fig. Visualization of community structures in Sapporo before node removal. $N = 1024$ nodes are located by the inverse order of population (Inv.). Different colors represent different communities estimated by Louvain method. There are different community formations compared to Figure S11 Fig..



S13 Fig. Increasing modularity Q vs. decreasing robustness index R^{RB} or critical fraction q_c^{RB} for varying the size N in Tokyo RNG networks.



S14 Fig. Increasing modularity Q vs. decreasing robustness index R^{RB} or critical fraction q_c^{RB} for varying the size N in Tokyo GG networks.

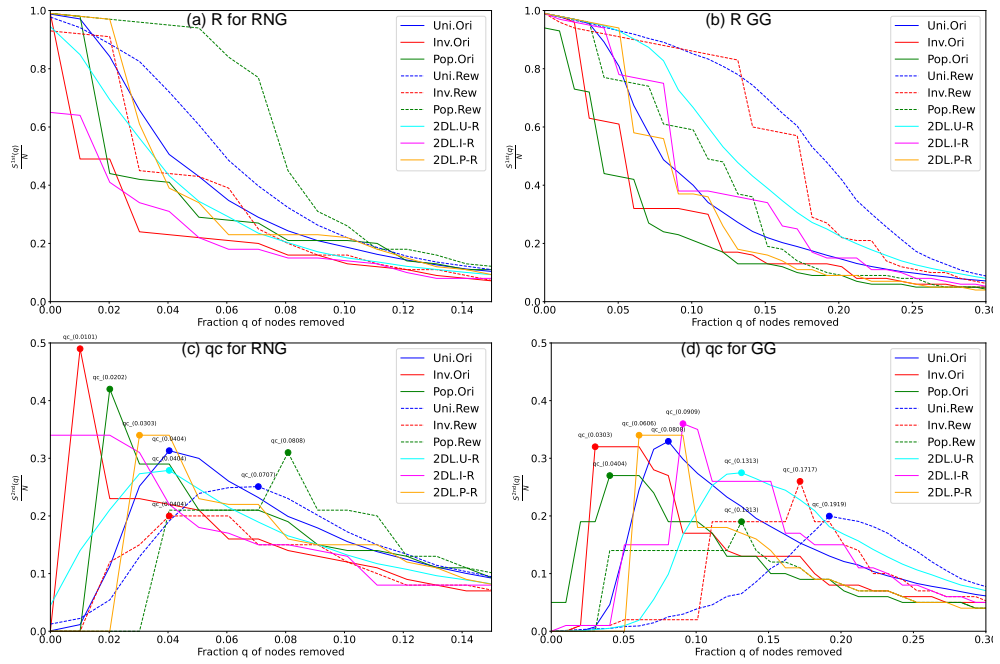


S15 Fig. Scatter plots show relation between network robustness measures (a for R and b for q_c) and the proportion of grid-like parts against random failures (RF). Networks with $N = 1024$ nodes are considered, where Pop. networks (green) show notably higher proportions of grid-like parts compared to Inv. (red) and Uni. (blue) networks. See the text at the end of subsection 3.3 for the detail.

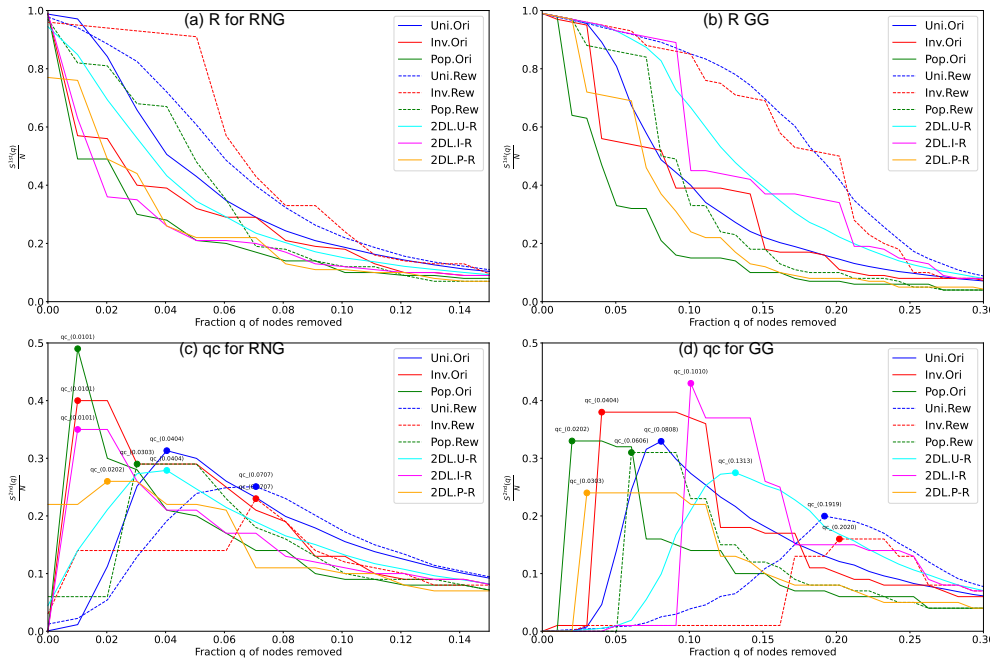
.3 Q,R and q_c relations

.4 scatters of Q vs R or q_c

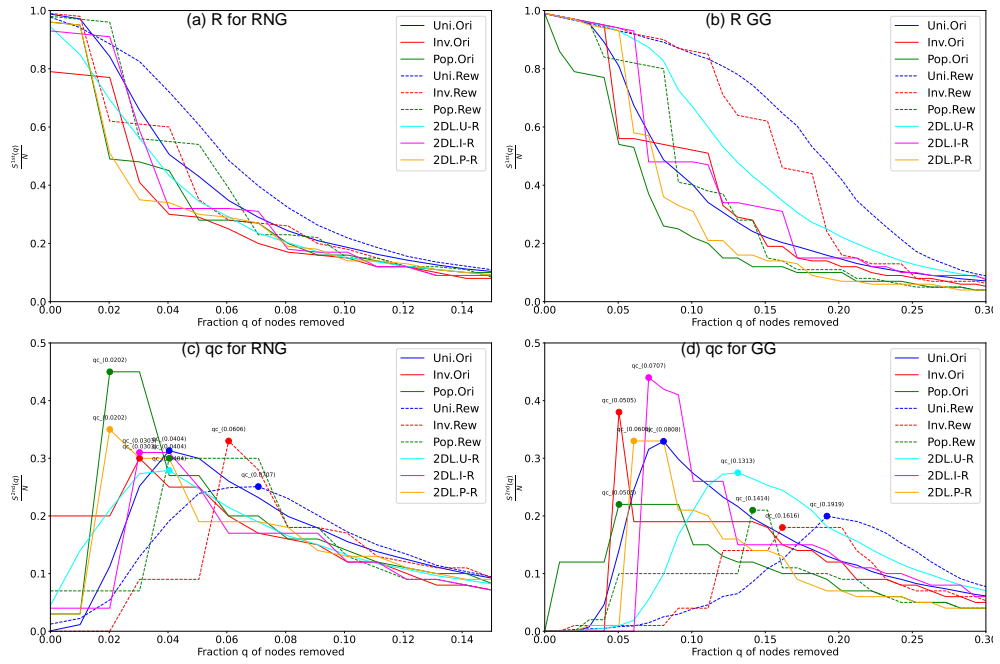
.5 Robustness against RB attacks



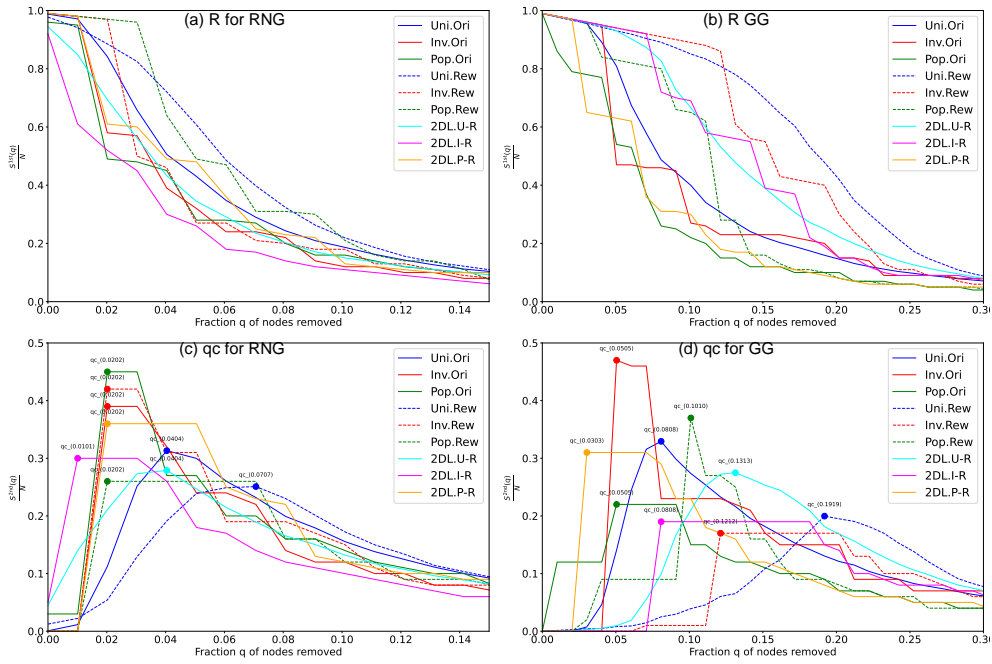
S16 Fig. Robustness against recalculated betweenness (RB) attacks for Fukuoka networks with $N = 100$ nodes. For both Rew (Randomized networks) and 2DL lines, the rewiring process preserves the original degree distributions. Two measures are applied: (a) (b) $S^1(q)/N$ the relative size of largest connected component, and (c) (d) $S^2(q)/N$ the critical fraction q_c at the peak of the relative size of second largest component.



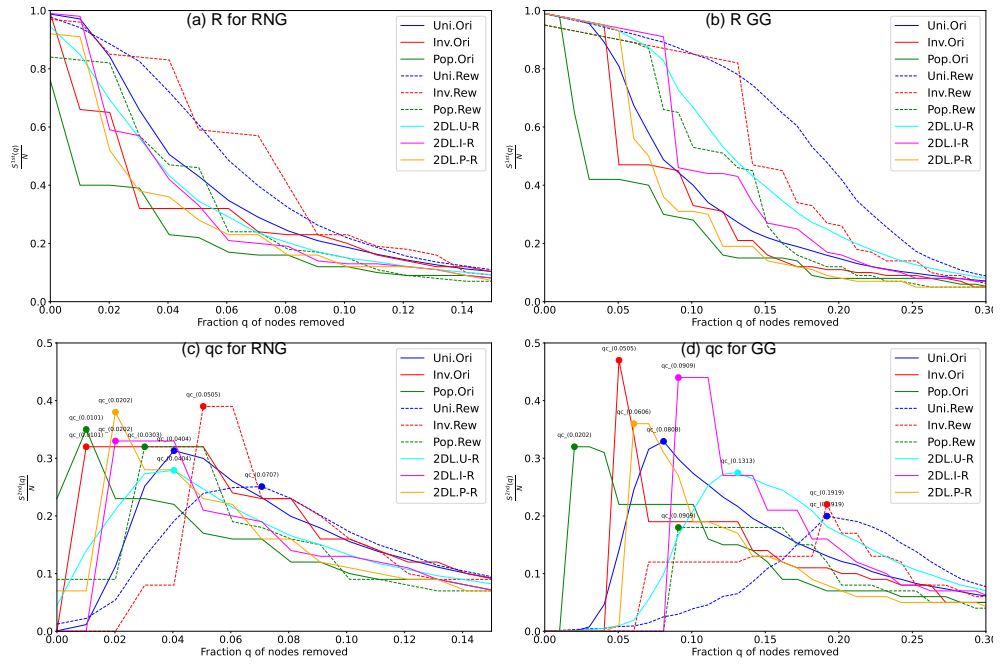
S17 Fig. Robustness against recalculated betweenness (RB) attacks for Hiroshima networks with $N = 100$ nodes. For both Rew (Randomized networks) and 2DL lines, the rewiring process preserves the original degree distributions. Two measures are applied: (a) (b) $S^{1st}(q)/N$ the relative size of largest connected component, and (c) (d) $S^{2nd}(q)/N$ the critical fraction q_c at the peak of the relative size of second largest component.



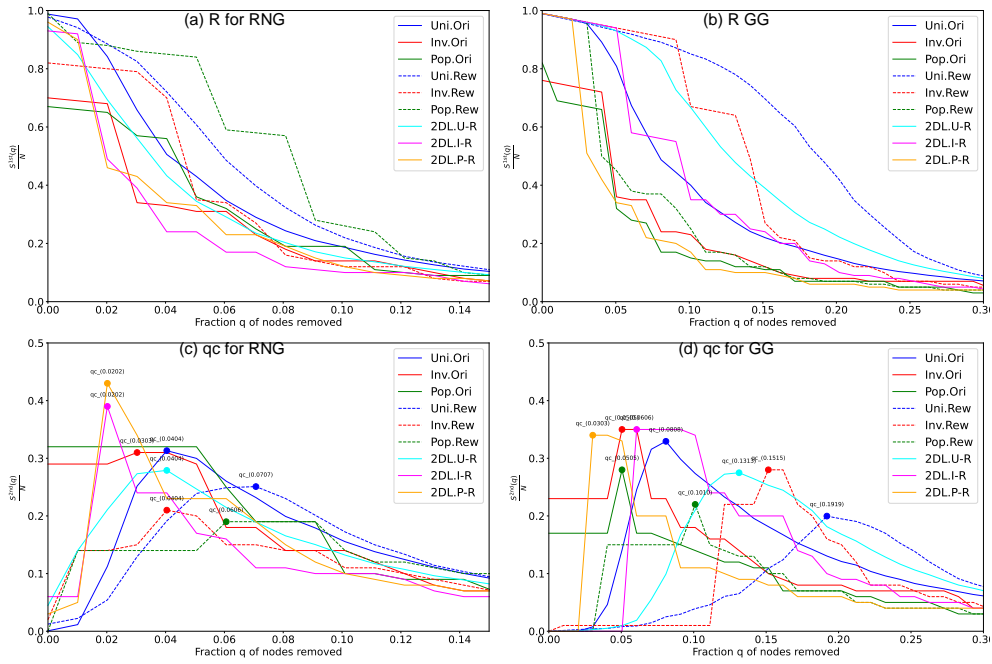
S18 Fig. Robustness against recalculated betweenness (RB) attacks for Keihan networks with $N = 100$ nodes. For both Rew (Randomized networks) and 2DL lines, the rewiring process preserves the original degree distributions. Two measures are applied: (a) (b) $S^{1st}(q)/N$ the relative size of largest connected component, and (c) (d) $S^{2nd}(q)/N$ the critical fraction q_c at the peak of the relative size of second largest component.



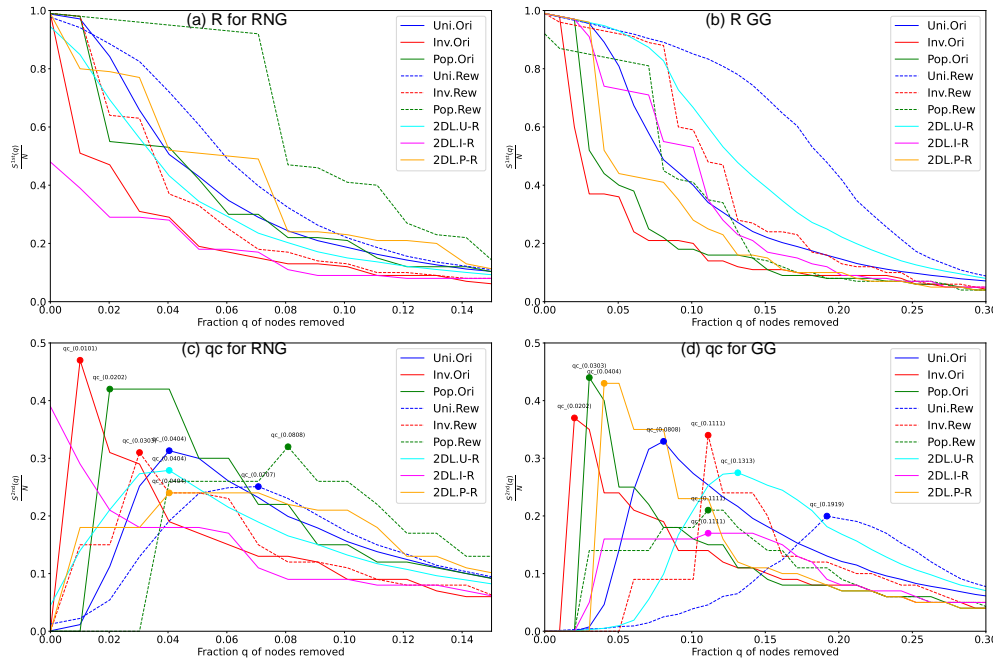
S19 Fig. Robustness against recalculated betweenness (RB) attacks for Nagoya networks with $N = 100$ nodes. For both Rew (Randomized networks) and 2DL lines, the rewiring process preserves the original degree distributions. Two measures are applied: (a) (b) $S^{1st}(q)/N$ the relative size of largest connected component, and (c) (d) $S^{2nd}(q)/N$ the critical fraction q_c at the peak of the relative size of second largest component.



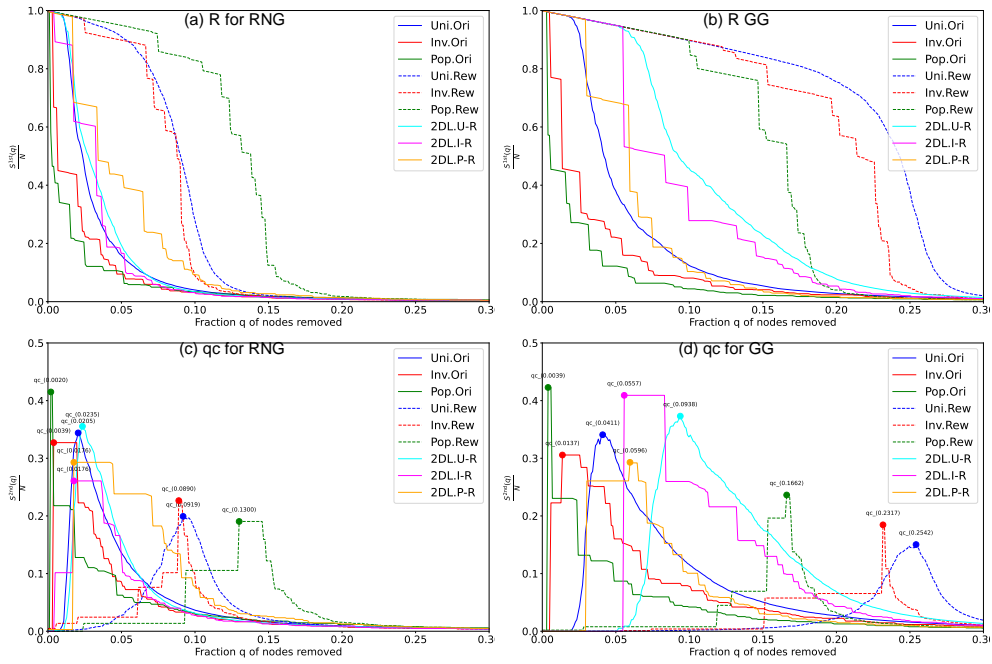
S20 Fig. Robustness against recalculated betweenness (RB) attacks for Tokyo networks with $N = 100$ nodes. For both Rew (Randomized networks) and 2DL lines, the rewiring process preserves the original degree distributions. Two measures are applied: (a) (b) $S^{1st}(q)/N$ the relative size of largest connected component, and (c) (d) $S^{2nd}(q)/N$ the critical fraction q_c at the peak of the relative size of second largest component.



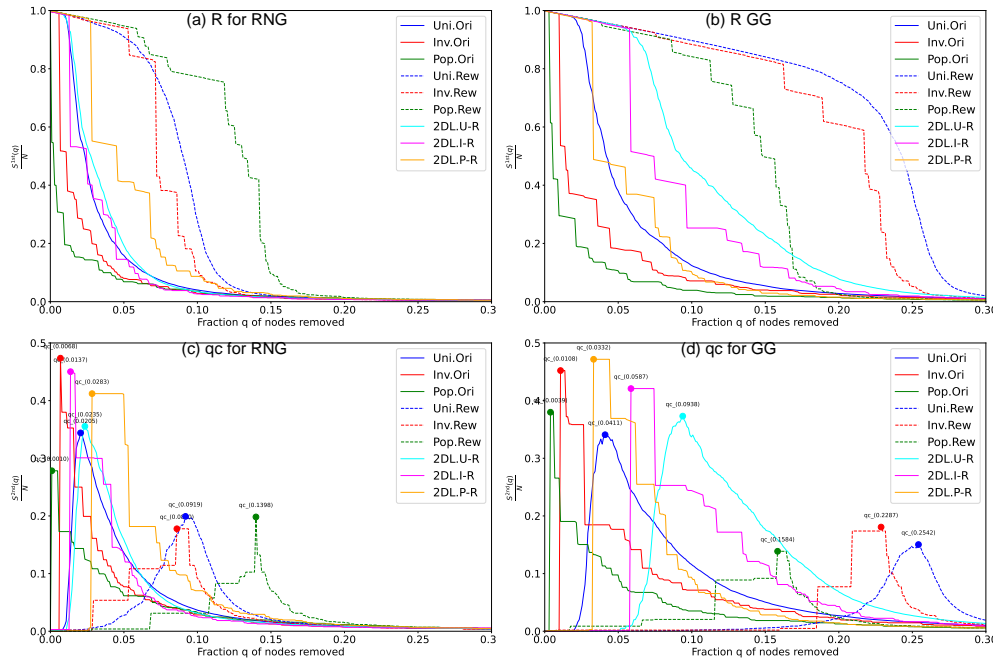
S21 Fig. Robustness against recalculated betweenness (RB) attacks for Sendai networks with $N = 100$ nodes. For both Rew (Randomized networks) and 2DL lines, the rewiring process preserves the original degree distributions. Two measures are applied: (a) (b) $S^{1st}(q)/N$ the relative size of largest connected component, and (c) (d) $S^{2nd}(q)/N$ the critical fraction q_c at the peak of the relative size of second largest component.



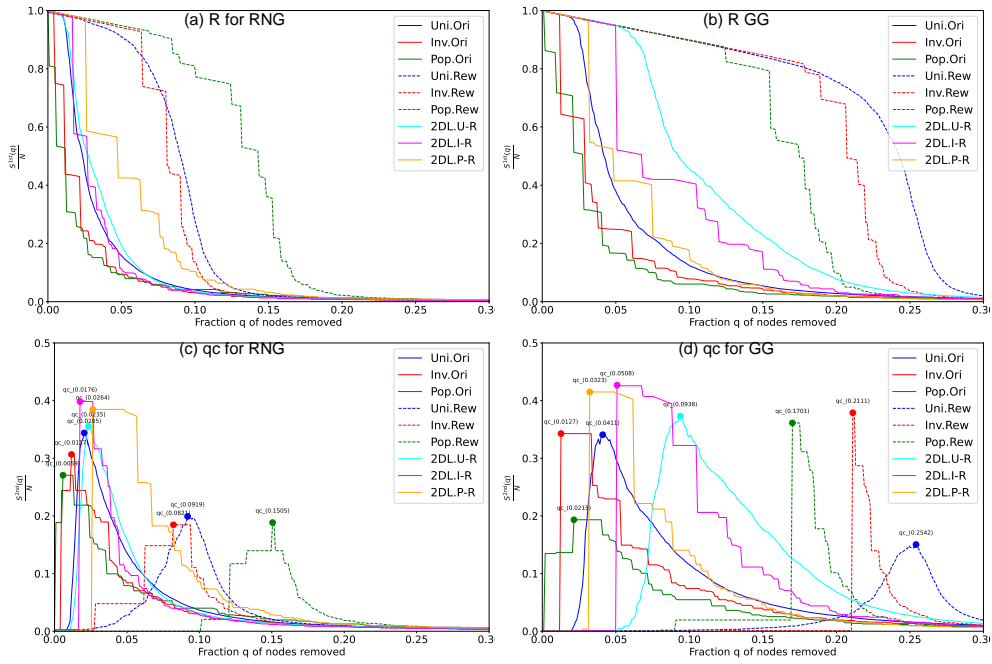
S22 Fig. Robustness against recalculated betweenness (RB) attacks for Sapporo networks with $N = 100$ nodes. For both Rew (Randomized networks) and 2DL lines, the rewiring process preserves the original degree distributions. Two measures are applied: (a) (b) $S^1(q)/N$ the relative size of largest connected component, and (c) (d) $S^2(q)/N$ the critical fraction q_c at the peak of the relative size of second largest component.



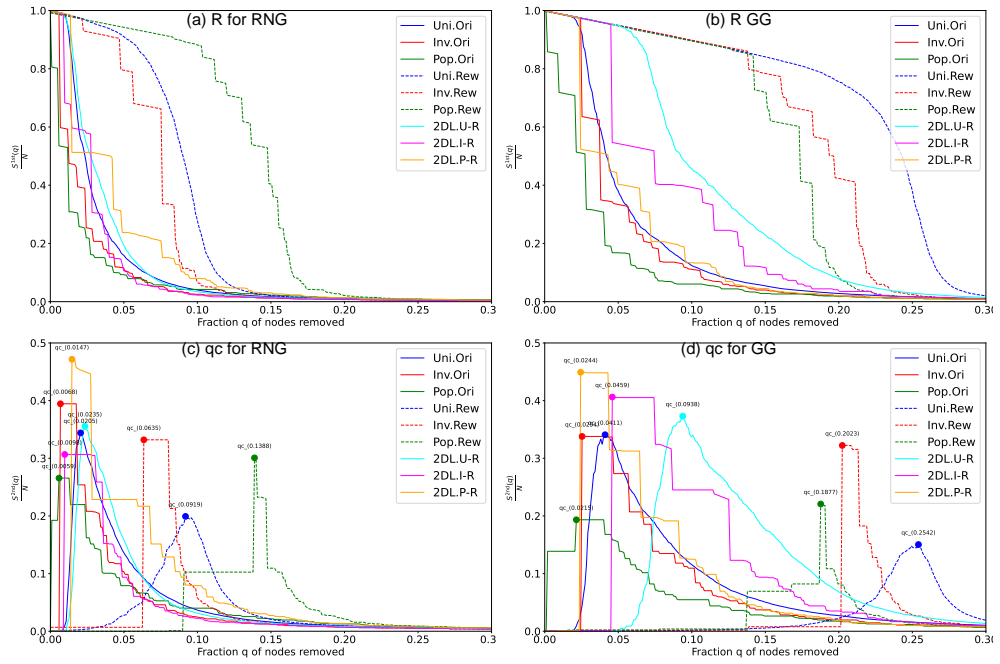
S23 Fig. Robustness against recalculated betweenness (RB) attacks for Fukuoka networks with $N = 1024$ nodes. For both Rew (Randomized networks) and 2DL lines, the rewiring process preserves the original degree distributions. Two measures are applied: (a) (b) $S^{1st}(q)/N$ the relative size of largest connected component, and (c) (d) $S^{2nd}(q)/N$ the critical fraction q_c at the peak of the relative size of second largest component.



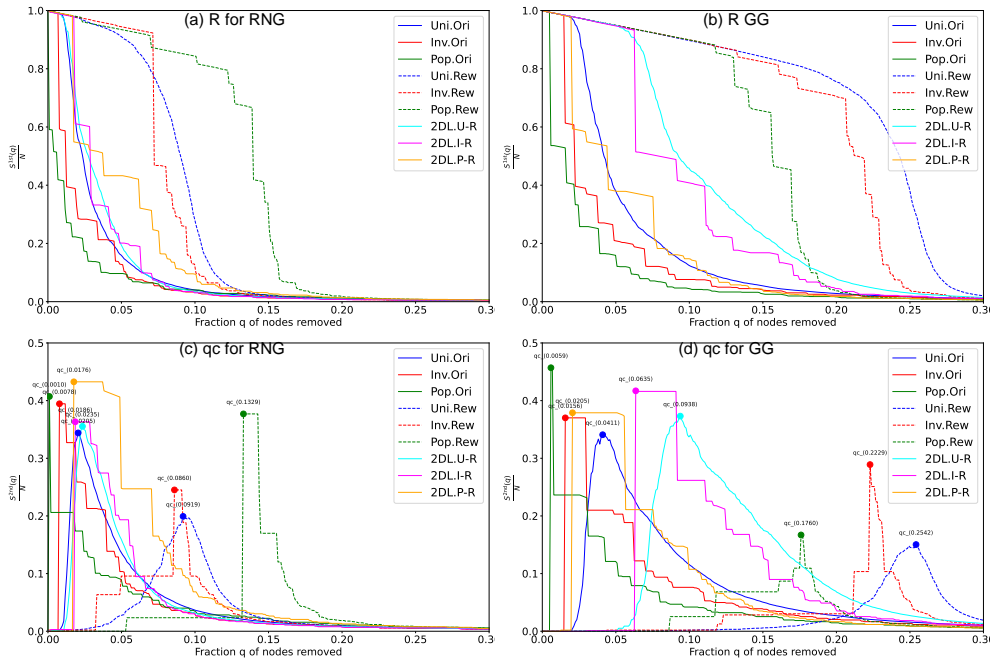
S24 Fig. Robustness against recalculated betweenness (RB) attacks for Hiroshima networks with $N = 1024$ nodes. For both Rew (Randomized networks) and 2DL lines, the rewiring process preserves the original degree distributions. Two measures are applied: (a) (b) $S^{1st}(q)/N$ the relative size of largest connected component, and (c) (d) $S^{2nd}(q)/N$ the critical fraction q_c at the peak of the relative size of second largest component.



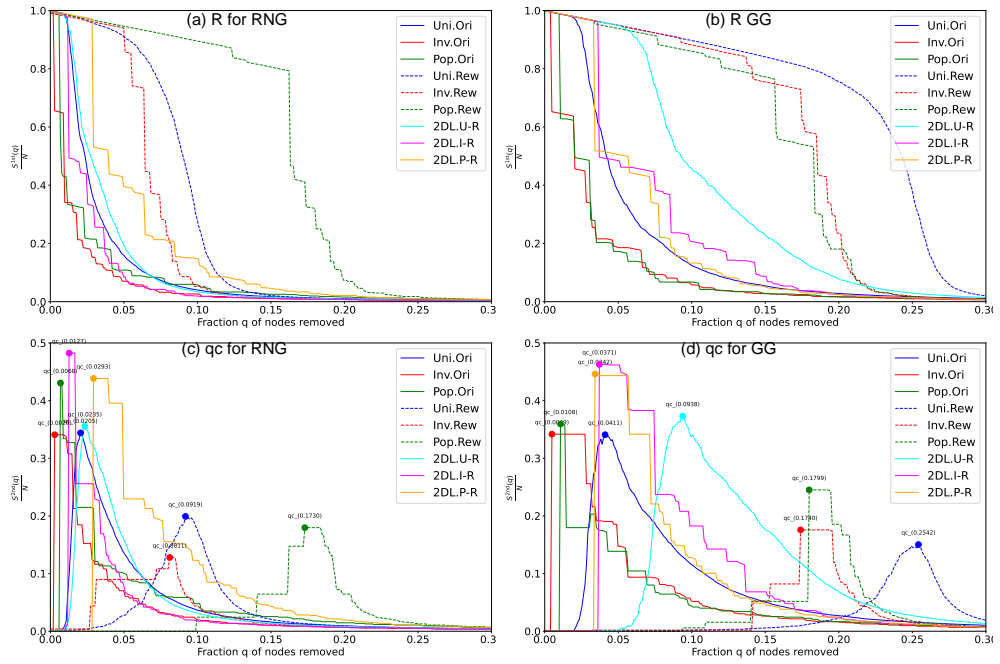
S25 Fig. Robustness against recalculated betweenness (RB) attacks for Keihan networks with $N = 1024$ nodes. For both Rew (Randomized networks) and 2DL lines, the rewiring process preserves the original degree distributions. Two measures are applied: (a) (b) $S^{1st}(q)/N$ the relative size of largest connected component, and (c) (d) $S^{2nd}(q)/N$ the critical fraction q_c at the peak of the relative size of second largest component.



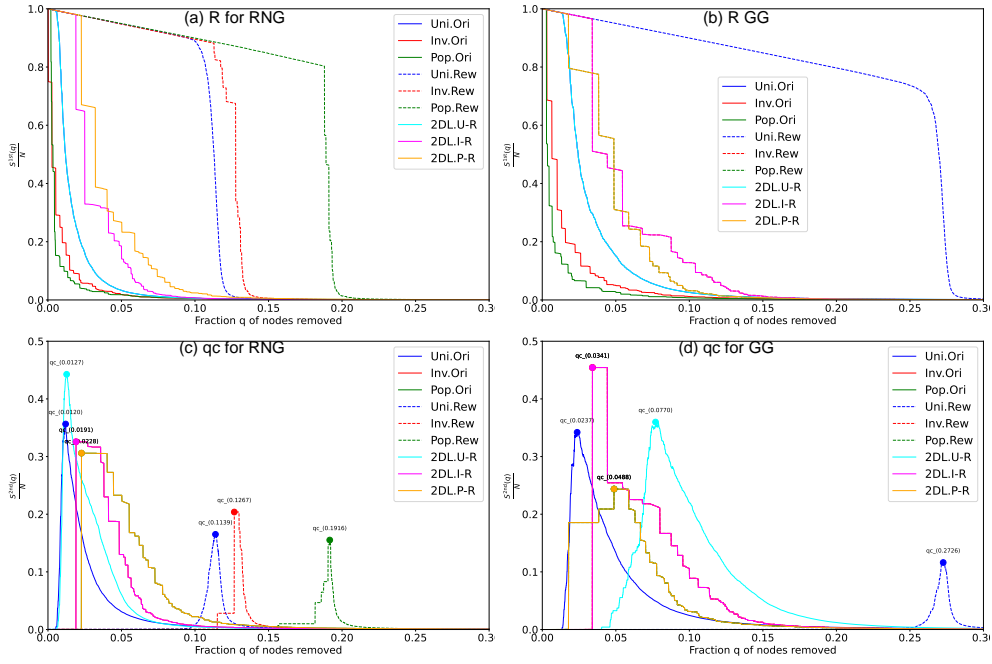
S26 Fig. Robustness against recalculated betweenness (RB) attacks for Nagoya networks with $N = 1024$ nodes. For both Rew (Randomized networks) and 2DL lines, the rewiring process preserves the original degree distributions. Two measures are applied: (a) (b) $S^{1st}(q)/N$ the relative size of largest connected component, and (c) (d) $S^{2nd}(q)/N$ the critical fraction q_c at the peak of the relative size of second largest component.



S27 Fig. Robustness against recalculated betweenness (RB) attacks for Sendai networks with $N = 1024$ nodes. For both Rew (Randomized networks) and 2DL lines, the rewiring process preserves the original degree distributions. Two measures are applied: (a) (b) $S^{1st}(q)/N$ the relative size of largest connected component, and (c) (d) $S^{2nd}(q)/N$ the critical fraction q_c at the peak of the relative size of second largest component.



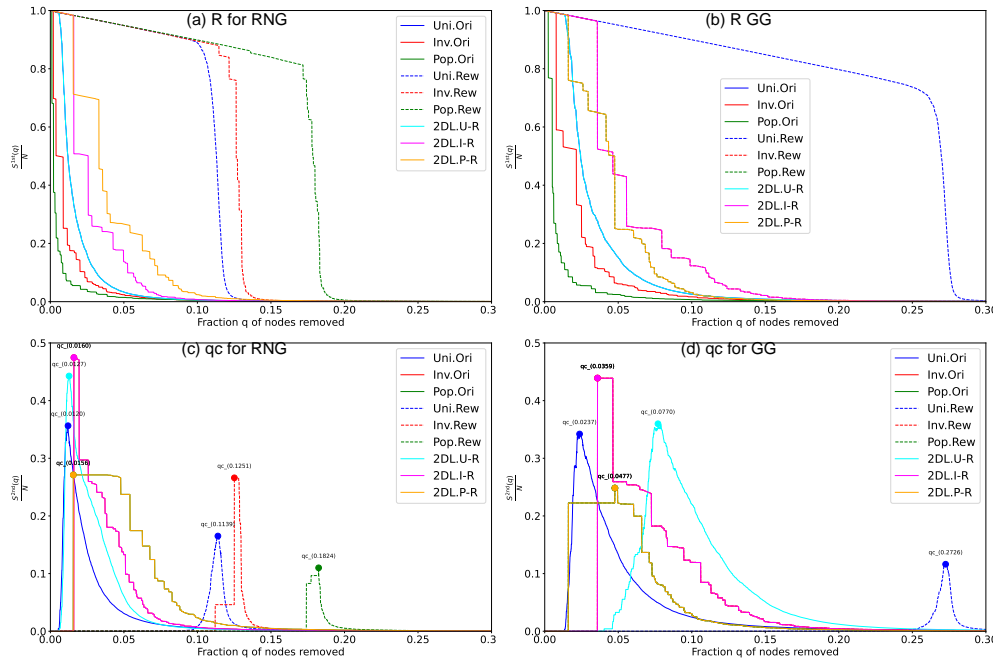
S28 Fig. Robustness against recalculated betweenness (RB) attacks for Sapporo networks with $N = 1024$ nodes. For both Rew (Randomized networks) and 2DL lines, the rewiring process preserves the original degree distributions. Two measures are applied: (a) (b) $S^{1st}(q)/N$ the relative size of largest connected component, and (c) (d) $S^{2nd}(q)/N$ the critical fraction q_c at the peak of the relative size of second largest component.



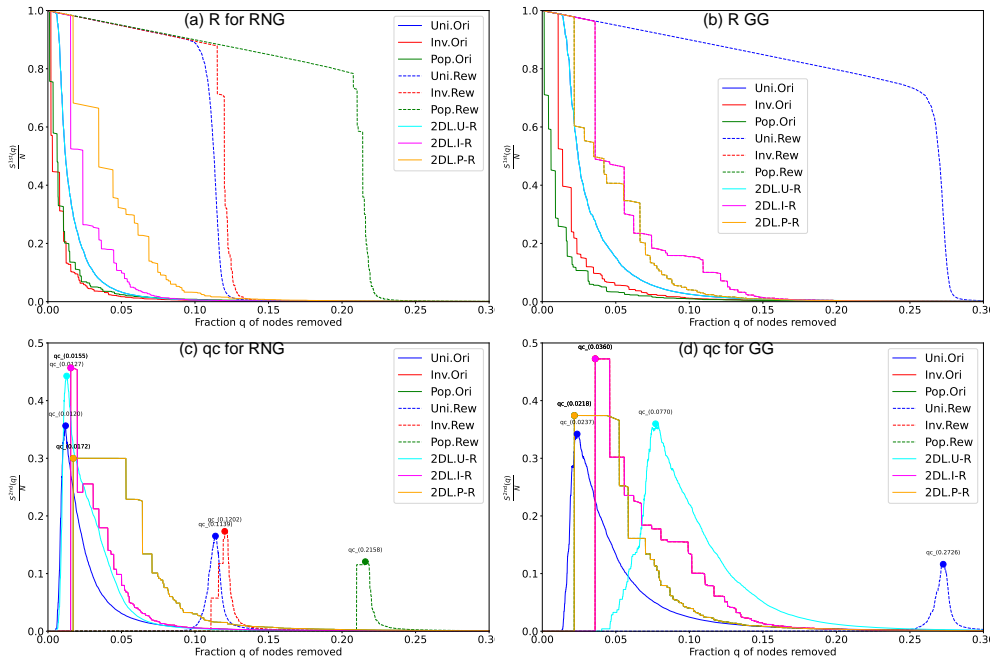
S29 Fig. Robustness against recalculated betweenness (RB) attacks for Fukuoka networks with $N = 10000$ nodes. For both Rew (Randomized networks) and 2DL lines, the rewiring process preserves the original degree distributions. Two measures are applied: (a) (b) $S^{1st}(q)/N$ the relative size of largest connected component, and (c) (d) $S^{2nd}(q)/N$ the critical fraction q_c at the peak of the relative size of second largest component.

.6 R to Q scatters

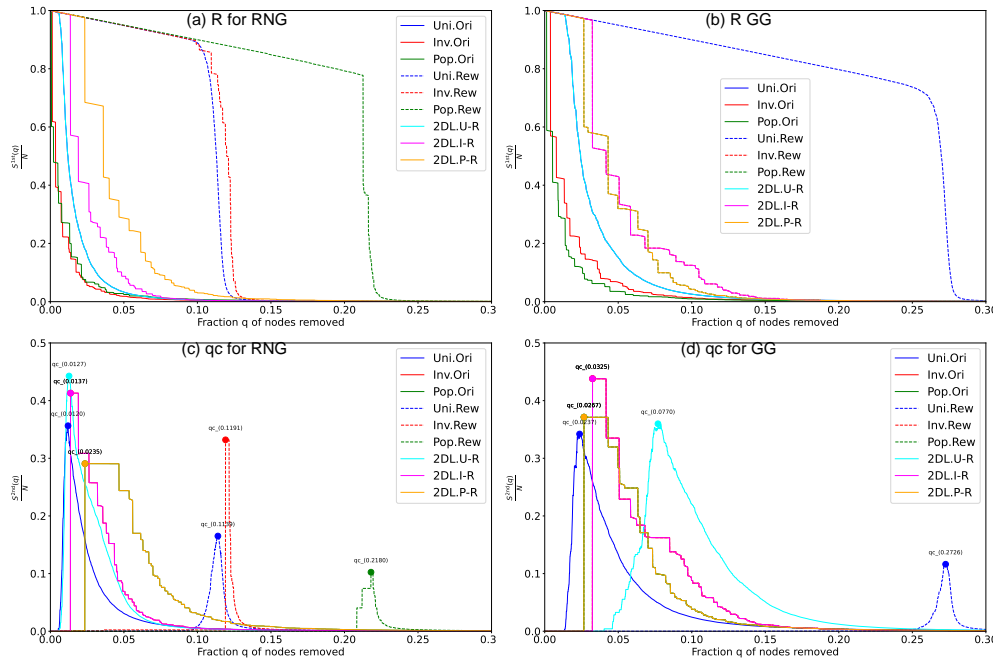
.7 tables



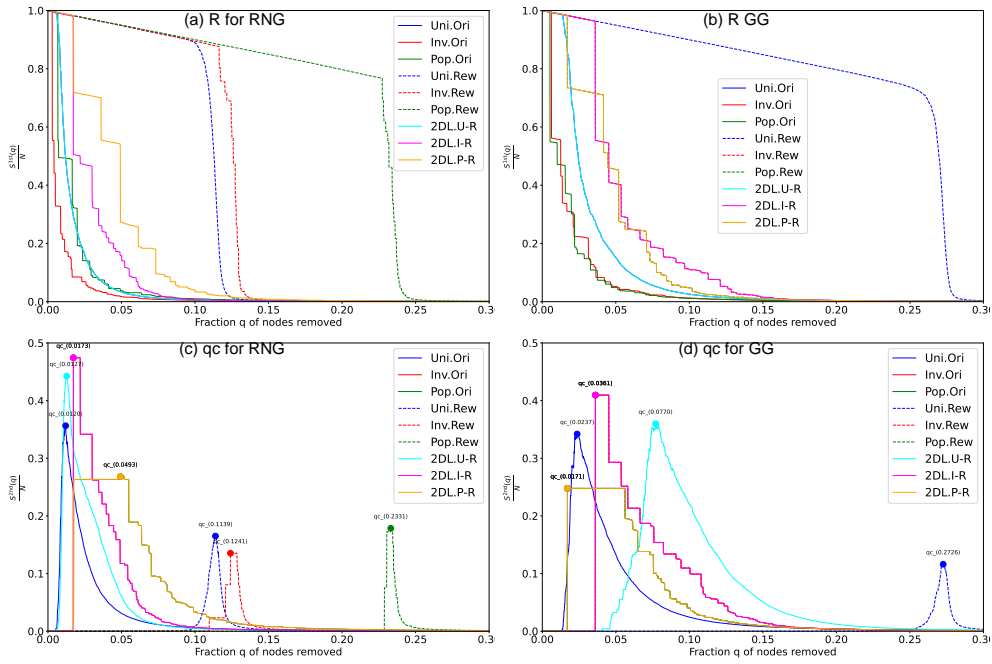
S30 Fig. Robustness against recalculated betweenness (RB) attacks for Hiroshima networks with $N = 10000$ nodes. For both Rew (Randomized networks) and 2DL lines, the rewiring process preserves the original degree distributions. Two measures are applied: (a) (b) $S^{1st}(q)/N$ the relative size of largest connected component, and (c) (d) $S^{2nd}(q)/N$ the critical fraction q_c at the peak of the relative size of second largest component.



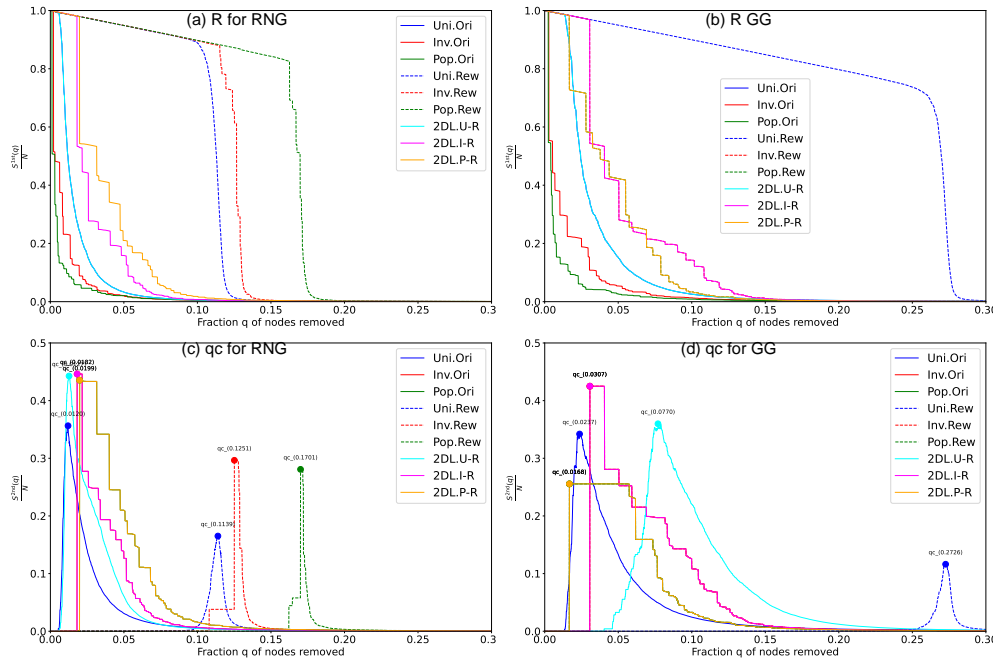
S31 Fig. Robustness against recalculated betweenness (RB) attacks for Keihan networks with $N = 10000$ nodes. For both Rew (Randomized networks) and 2DL lines, the rewiring process preserves the original degree distributions. Two measures are applied: (a) (b) $S^{1st}(q)/N$ the relative size of largest connected component, and (c) (d) $S^{2nd}(q)/N$ the critical fraction q_c at the peak of the relative size of second largest component.



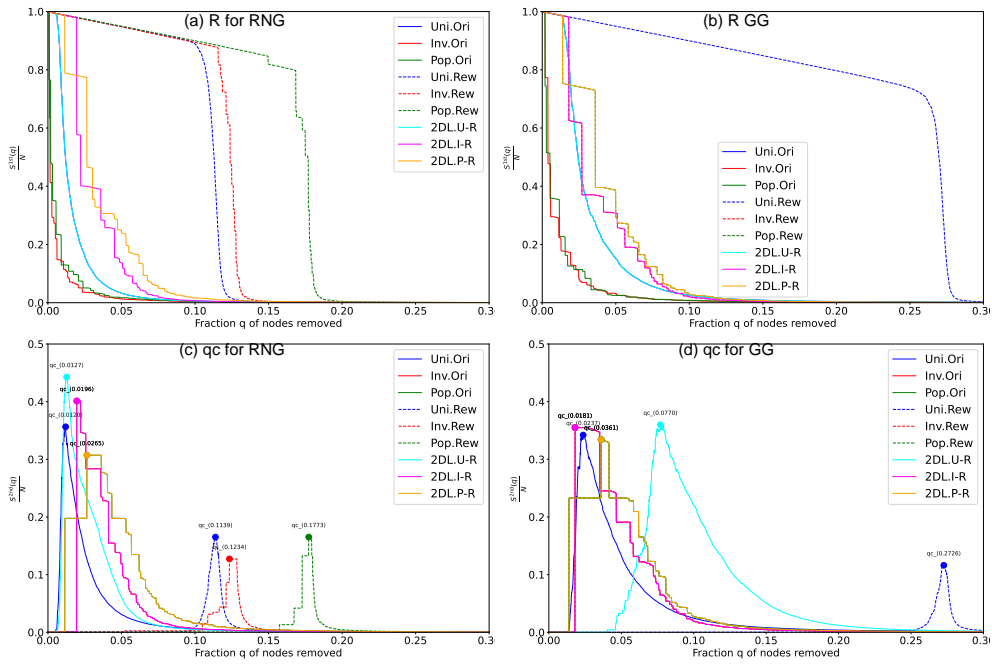
S32 Fig. Robustness against recalculated betweenness (RB) attacks for Nagoya networks with $N = 10000$ nodes. For both Rew (Randomized networks) and 2DL lines, the rewiring process preserves the original degree distributions. Two measures are applied: (a) (b) $S^{1st}(q)/N$ the relative size of largest connected component, and (c) (d) $S^{2nd}(q)/N$ the critical fraction q_c at the peak of the relative size of second largest component.



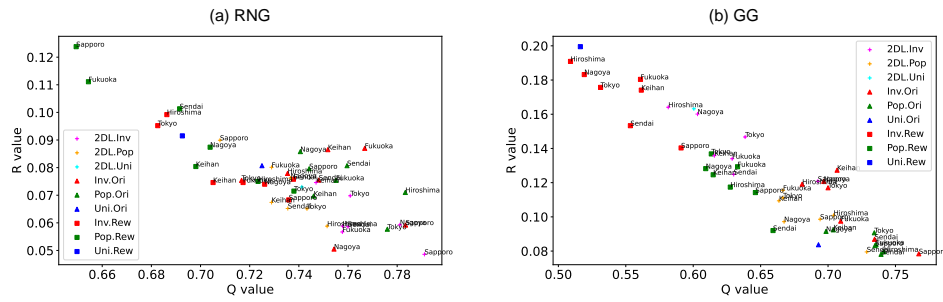
S33 Fig. Robustness against recalculated betweenness (RB) attacks for Tokyo networks with $N = 10000$ nodes. For both Rew (Randomized networks) and 2DL lines, the rewiring process preserves the original degree distributions. Two measures are applied: (a) (b) $S^{1st}(q)/N$ the relative size of largest connected component, and (c) (d) $S^{2nd}(q)/N$ the critical fraction q_c at the peak of the relative size of second largest component.



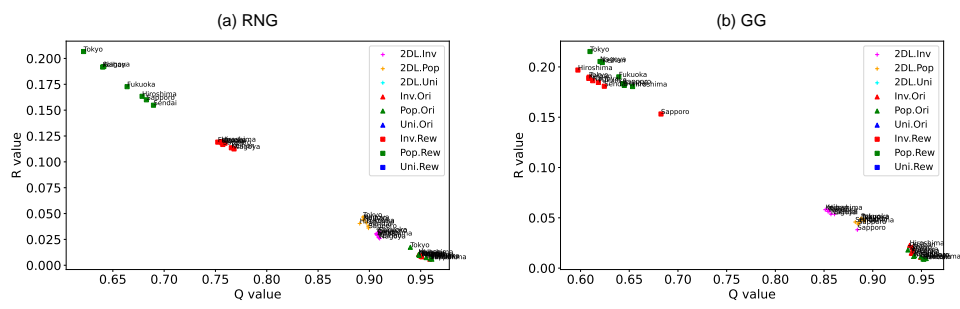
S34 Fig. Robustness against recalculated betweenness (RB) attacks for Sendai networks with $N = 10000$ nodes. For both Rew (Randomized networks) and 2DL lines, the rewiring process preserves the original degree distributions. Two measures are applied: (a) (b) $S^{1st}(q)/N$ the relative size of largest connected component, and (c) (d) $S^{2nd}(q)/N$ the critical fraction q_c at the peak of the relative size of second largest component.



S35 Fig. Robustness against recalculated betweenness (RB) attacks for Sapporo networks with $N = 10000$ nodes. For both Rew (Randomized networks) and 2DL lines, the rewiring process preserves the original degree distributions. Two measures are applied: (a) (b) $S^{1st}(q)/N$ the relative size of largest connected component, and (c) (d) $S^{2nd}(q)/N$ the critical fraction q_c at the peak of the relative size of second largest component.



S36 Fig. Relation between robustness index R^{RB} and modularity Q in networks with $N = 100$ nodes



S37 Fig. Relation between robustness index R^{RB} and modularity Q in networks with $N = 10000$ nodes

Cities	R^{RB}				q_c^{RB}			
	RNG		GG		RNG		GG	
	Inv.	Pop.	Inv.	Pop.	Inv.	Pop.	Inv.	Pop.
Fukuoka	0.0870 Δ	0.0754 ∇	0.0975 Δ	0.0837	0.0101 ∇	0.0202 ∇	0.0303 ∇	0.0404 ∇
Hiroshima	0.0779 ∇	0.0710 ∇	0.1191 Δ	0.0796 ∇	0.0101 ∇	0.0101 ∇	0.0404 ∇	0.0202 ∇
Keihan	0.0865 Δ	0.0697 ∇	0.1273 Δ	0.0924 Δ	0.0303 ∇	0.0202 ∇	0.0505 ∇	0.0505 ∇
Nagoya	0.0505 ∇	0.0858 Δ	0.1208 Δ	0.0915 Δ	0.0202 ∇	0.0202 ∇	0.0505 ∇	0.0505 ∇
Tokyo	0.0754 ∇	0.0577 ∇	0.1170 Δ	0.0907 Δ	0.0101 ∇	0.0101 ∇	0.0505 ∇	0.0202 ∇
Sendai	0.0755 ∇	0.0807	0.0869 Δ	0.0781 ∇	0.0303 ∇	0.0000 ∇	0.0505 ∇	0.0505 ∇
Sapporo	0.0592 ∇	0.0796 ∇	0.0784 ∇	0.0832 ∇	0.0101 ∇	0.0202 ∇	0.0202 ∇	0.0303 ∇
Uniform	0.0807		0.0837		0.0404		0.0808	
2D Lattice	0.1636				0.0909			

S1 Table Robustness index (R^{RB}) and Critical fraction (q_c^{RB}) against Recalculated Betweenness (RB) attacks in networks with $N = 100$ nodes for seven major Japanese areas. Higher values indicate greater robustness of connectivity. For R^{RB} , values with upper-triangles (Δ) indicate higher robustness than Uni. case, while values with lower-triangles (∇) indicate lower robustness than Uni. case. For q_c^{RB} , all values are marked with lower-triangles (∇) as they show lower robustness than Uni. case.

Cities	R^{RB}				q_c^{RB}			
	RNG		GG		RNG		GG	
	Inv.	Pop.	Inv.	Pop.	Inv.	Pop.	Inv.	Pop.
Fukuoka	0.0237 ∇	0.0188 ∇	0.0379 ∇	0.0253 ∇	0.0039 ∇	0.0020 ∇	0.0137 ∇	0.0039 ∇
Hiroshima	0.0234 ∇	0.0162 ∇	0.0379 ∇	0.0219 ∇	0.0068 ∇	0.0010 ∇	0.0108 ∇	0.0039 ∇
Keihan	0.0258 ∇	0.0232 ∇	0.0448 ∇	0.0375 ∇	0.0117 ∇	0.0059 ∇	0.0127 ∇	0.0215 ∇
Nagoya	0.0262 ∇	0.0233 ∇	0.0548 ∇	0.0370 ∇	0.0068 ∇	0.0059 ∇	0.0254 ∇	0.0215 ∇
Tokyo	0.0271 ∇	0.0284 ∇	0.0486 ∇	0.0446 ∇	0.0098 ∇	0.0059 ∇	0.0235 ∇	0.0205 ∇
Sendai	0.0271 ∇	0.0199 ∇	0.0433 ∇	0.0292 ∇	0.0078 ∇	0.0010 ∇	0.0156 ∇	0.0059 ∇
Sapporo	0.0200 ∇	0.0264 ∇	0.0356 ∇	0.0369 ∇	0.0029 ∇	0.0068 ∇	0.0049 ∇	0.0108 ∇
Uniform	0.0350		0.0620		0.0205		0.0411	
2D Lattice	0.0677				0.0303			

S2 Table Robustness index (R^{RB}) and Critical fraction (q_c^{RB}) against Recalculated Betweenness (RB) attacks in networks with $N = 1024$ nodes for seven major Japanese areas. Higher values indicate greater robustness of connectivity. Values with lower-triangles (∇) indicate where the cases of Pop. and Inv. have lower robustness of connectivity than the cases of Uni. for both RNG and GG.

Cities	R^{RB}				q_c^{RB}			
	RNG		GG		RNG		GG	
	Inv.	Pop.	Inv.	Pop.	Inv.	Pop.	Inv.	Pop.
Fukuoka	0.0082 ∇	0.0070 ∇	0.0149 ∇	0.0091 ∇	0.0028 ∇	0.0045 ∇	0.0032 ∇	0.0029 ∇
Hiroshima	0.0106 ∇	0.0059 ∇	0.0227 ∇	0.0095 ∇	0.0021 ∇	0.0011 ∇	0.0079 ∇	0.0052 ∇
Keihan	0.0090 ∇	0.0105 ∇	0.0208 ∇	0.0123 ∇	0.0021 ∇	0.0012 ∇	0.0109 ∇	0.0014 ∇
Nagoya	0.0086 ∇	0.0095 ∇	0.0166 ∇	0.0116 ∇	0.0014 ∇	0.0008 ∇	0.0040 ∇	0.0014 ∇
Tokyo	0.0092 ∇	0.0174 ∇	0.0189 ∇	0.0180 ∇	0.0030 ∇	0.0068 ∇	0.0063 ∇	0.0053 ∇
Sendai	0.0094 ∇	0.0063 ∇	0.0146 ∇	0.0089 ∇	0.0022 ∇	0.0012 ∇	0.0029 ∇	0.0025 ∇
Sapporo	0.0059 ∇	0.0074 ∇	0.0108 ∇	0.0112 ∇	0.0011 ∇	0.0019 ∇	0.0039 ∇	0.0019 ∇
Uniform	0.0173		0.0334		0.0115		0.0229	
2D Lattice	0.0647				0.0679			

S3 Table Robustness index (R^{RB}) and Critical fraction (q_c^{RB}) against Recalculated Betweenness (RB) attacks in networks with $N = 10000$ nodes for seven major Japanese areas. Higher values indicate greater robustness of connectivity. Values with lower-triangles (∇) indicate where the cases of Pop. and Inv. have lower robustness of connectivity than the cases of Uni. for both RNG and GG.

Cities	RNG		GG	
	Inv.	Pop.	Inv.	Pop.
Fukuoka	2.28	2.5	3.14	2.72
Hiroshima	2.34	2.24	3.52	2.6
Keihan	2.3	2.34	3.34	2.82
Nagoya	2.26	2.34	3.36	2.82
Tokyo	2.36	2.24	3.38	2.8
Sendai	2.24	2.38 Δ	3.14	2.5
Sapporo	2.18	2.54	2.92	2.62
Uniform	2.37		3.56	
2D Lattice	3.6			

S4 Table Average degree ($\langle k \rangle$) in networks with (N) = 100 nodes for seven major Japanese areas. Higher average degrees mean more links per node in the network. Values with upper-triangles (Δ) indicate where the cases of Pop. and Inv. have higher $\langle k \rangle$ than the cases of Uni. for both RNG and GG.

Cities	RNG		GG	
	Inv.	Pop.	Inv.	Pop.
Fukuoka	2.67 [△]	3.07 [△]	3.35	3.21
Hiroshima	2.66 [△]	3.01 [△]	3.49	3.14
Keihan	2.62 [△]	3.21 [△]	3.39	3.32
Nagoya	2.61 [△]	3.21 [△]	3.38	3.33
Tokyo	2.65 [△]	3.32 [△]	3.42	3.41
Sendai	2.66 [△]	2.95 [△]	3.31	3.19
Sapporo	2.66 [△]	2.99 [△]	2.99	3.19
Uniform	2.54		3.96	
2D Lattice	3.96			

S5 Table Average degree $\langle k \rangle$ in networks with $(N) = 10000$ nodes for seven major Japanese areas. Higher average degrees mean more links per node in the network. Values with upper-triangles (Δ) indicate where the cases of Pop. and Inv. have higher $\langle k \rangle$ than the cases of Uni. for both RNG and GG.

Cities	RNG		GG	
	Inv.	Pop.	Inv.	Pop.
Fukuoka	0.7668 [△]	0.7551 [△]	0.7094 [△]	0.7356 [△]
Hiroshima	0.7354 [△]	0.7833 [△]	0.6808 [▽]	0.7414 [△]
Keihan	0.7518 [△]	0.746 [△]	0.7067 [△]	0.7039 [△]
Nagoya	0.7543 [△]	0.7406 [△]	0.6968 [△]	0.6985 [△]
Tokyo	0.7167 [▽]	0.776 [△]	0.7 [△]	0.7343 [△]
Sendai	0.7481 [△]	0.7596 [△]	0.7345 [△]	0.7393 [△]
Sapporo	0.7834 [△]	0.7442 [△]	0.7673 [△]	0.7348 [△]
Uniform	0.725		0.6929	

S6 Table Modularity Q in networks with 100 nodes for seven major Japanese areas. Higher values indicate stronger community structures. Values with upper-triangles (Δ) or lower-triangles (∇) indicate where the cases of Pop. and Inv. have higher or lower modularity than the case of Uni. for both RNG and GG. Note the generally higher modularity in Pop. and Inv. compared to Uni. networks for both RNG and GG.

Cities	RNG		GG	
	Inv.	Pop.	Inv.	Pop.
Fukuoka	0.9514 [△]	0.9603 [△]	0.9395 [△]	0.9516 [△]
Hiroshima	0.948 [△]	0.9609 [△]	0.9379 [△]	0.9549 [△]
Keihan	0.9509 [△]	0.9481 [△]	0.9406 [△]	0.9429 [△]
Nagoya	0.9506 [△]	0.9485 [△]	0.9406 [△]	0.942 [△]
Tokyo	0.9499 [△]	0.9399 [△]	0.9411 [△]	0.9361 [△]
Sendai	0.9508 [△]	0.9594 [△]	0.9406 [△]	0.9525 [△]
Sapporo	0.9589 [△]	0.9553 [△]	0.9492 [△]	0.9495 [△]
Uniform	0.9397		0.9303	

S7 Table Modularity Q in networks with 10000 nodes for seven major Japanese areas. Higher values indicate stronger community structures. Values with upper-triangles (\triangle) indicate where the cases of Pop. and Inv. have higher modularity than the case of Uni. for both RNG and GG. Note the generally higher modularity in Pop. and Inv. compared to Uni. networks for both RNG and GG.